Geothermics 128 (2025) 103272

Contents lists available at ScienceDirect

Geothermics

journal homepage: www.elsevier.com/locate/geothermics

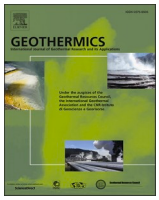

Geothermal resources in the northern Harrat Rahat volcanic field, Saudi Arabia: A drilling and field data assessment

Alan Bischoff [a,b,*], Khalid A. Bankher [c], Ehab A. Alashi [c], Teppo Arola [a], Haitham S. Brinji [c], Károly Németh [c,d], Annu Martinkauppi [a], Akram H. Jabrte [c], Evgenii Kortunov [a], Ibrahim S. Alzahrani [c], Ilkka Martinkauppi [a], Rami A. Melibari [c]

[a] Geological Survey of Finland (GTK), Vuorimiehentie 5, PO Box 96, Espoo 02151, Finland
[b] University of Turku, Akatemiankatu 1, Turku 20500, Finland
[c] Saudi Geological Survey (SGS), Al Waha, Jeddah 23352, Saudi Arabia
[d] Institute of Earth Physics and Space Science, Sopron, Hungary

ARTICLE INFO

Keywords:
Geothermal energy
Volcanostratigraphy
Harrat Rahat
Kingdom of Saudi Arabia
Geothermal assessment
Drilling

ABSTRACT

Geothermal energy exploration is gaining momentum in the Kingdom of Saudi Arabia. Here, we present the findings of a geothermal exploration programme conducted in the northern Harrat Rahat volcanic field. Our investigations highlight the geological events, volcanological characteristics, and structural patterns that influence the formation and distribution of geothermal resources in the area. The main objective was to identify conventional geothermal systems suitable for commercial electricity generation and secondarily estimate the potential of unconventional geothermal systems. Key findings include the recording of a modest conduction-dominated geothermal gradient of up to 23.6 °C/km. Although no active geothermal reservoirs were found (maximum measured temperature of 54 °C), the mineral paragenesis, including chlorite, epidote, and rhodonite associated with hydraulic brecciation, indicates that fossil high-temperature (~300 °C) hydrothermal systems were once working at shallow depths (<1000 m) beneath the Rahat. Accounting the uncertainties of our preliminary study, we estimate that unconventional geothermal systems could potentially achieve MWe-scale capacities if built at depths of nearly 6 km. The results of our research provide valuable insights into the geothermal potential of the Rahat volcanic field and contribute to expanding the understanding of geothermal resources in Saudi Arabia and similar geological settings worldwide.

1. Introduction

The production of geothermal energy is a mature technology, widely utilized across diverse socio-economic applications globally, including space heating and cooling, greenhouse farming, aquaculture, recreation, district heating networks, various industrial uses, and electricity generation. Driven by its diverse applications and low carbon footprint, the interest in geothermal heat is growing rapidly, particularly for its potential to accelerate our nation's energy transition goals with its high baseload power value.

In recent years, the Kingdom of Saudi Arabia has joined global efforts to unlock the next generation of clean energy sources vital for fueling our economy and society (e.g. Lashin et al. 2020; Kamboj et al., 2023). This paper presents the findings of a comprehensive geothermal exploration programme conducted by the Saudi Geological Survey (SGS) in collaboration with the Geological Survey of Finland (GTK) from September 2021 to December 2023. The research investigates the geothermal potential of key areas in central-west Saudi Arabia (Fig. 1). Studies carried out in the northern Harrat Rahat volcanic field (referred to as Rahat in this paper) focused on assessing the geothermal potential of an active volcanic area, making it the primary focus of this paper. In contrast, investigations of the heat-generating capacity and reservoir potential of granitic rocks were undertaken in the vicinity of the Rahat, with their findings reserved for forthcoming publications. Specifically, our paper explores the primary geological events, volcanological characteristics, and structural patterns that play a crucial role in shaping the formation and distribution of conventional geothermal plays in the Rahat. The main goal centered on identifying high-temperature (>200 °C) geothermal resources suitable for commercial electricity generation. Secondarily, we seek to estimate the geothermal potential of

* Corresponding author at: Geological Survey of Finland (GTK), Vuorimiehentie 5, PO Box 96, Espoo 02151, Finland.
E-mail address: alan.bischoff@utu.fi (A. Bischoff).

https://doi.org/10.1016/j.geothermics.2025.103272
Received 23 August 2024; Received in revised form 3 February 2025; Accepted 8 February 2025
Available online 13 February 2025

unconventional Enhanced Geothermal Systems (EGS) and Advanced Closed-Loop Systems (ACS), as well as explore complementary hybrid systems lower-temperature applications for geothermal resources in the study area.

This research programme has set the stage for a new momentum of geothermal exploration in the Kingdom of Saudi Arabia. For the first time, five exploration wells were successfully drilled to depths of ~1000 m, with the exclusive aim of assessing the geothermal potential of volcanic and granitic areas in the Saudi land. State-of-the-art geophysical data and detailed fieldwork mapping were employed to locate exploration targets for drilling. Temperature profiles were continuously recorded from all drillholes, and conceptual models were created to assess geothermal resources within the northern part of the Rahat. Our exploration programme has produced an invaluable wealth of data that will aid geologists, geophysicists, and the broader energy industry in evaluating Saudi Arabia's geothermal potential for years to come.

2. Geotectonic and geothermal settings of the Rahat volcanic field

The study area is situated in the central-western part of the Arabian Plate, characterized by the collage of accretionary Neoproterozoic island-arc terranes covered by Phanerozoic sedimentary deposits and Cenozoic lava fields (Camp and Roobol 1989; Stern and Johnson 2010). The Arabian Plate began to separate from the African Plate approximately 30 million years ago due to extension along the Red Sea and Gulf of Aden rifts (Bosworth 2015). Varied rates of extension along these rifts caused the Arabian plate to rotate counterclockwise, leading to its subsequent northward oblique continental collision with the Eurasian plate (Stern and Johnson 2010). The surface geology of the Arabian plate comprises two main domains. The western part consists mainly of Precambrian igneous and supracrustal basement rocks (Arabian Shield), which have been pierced and buried by late Cenozoic lava fields (locally referred to as "harrat", in Arabic meaning hot dark rock desert). In contrast, the eastern part is predominantly covered by Phanerozoic sedimentary strata related to the Tethyan passive margin evolution (Arabian Platform), which is home to many prime hydrocarbon fields (Fig. 1). Today, the Arabian Plate is bordered to the northeast by the Bitlis-Zagros suture zone alongside the Eurasian Plate, to the southwest and south by the Red Sea and the Gulf of Aden spreading centers, respectively, and to the northwest by the Dead Sea Transform Zone, adjacent to the northern African and eastern Anatolian Plates (Fig. 1). Overall, the crustal thickness of the Arabian Plate (depth to the Moho discontinuity) averages around 40 km, showing a gradual increase from 35 to 40 km in the Arabian Shield to 40–45 km beneath the eastern Arabian Platform (Mooney et al. 1985). This relatively thick crust poses challenges for geothermal exploration in the Kingdom of Saudi Arabia due to the relatively low heat flow of the region (Lucazeau 2019).

The Arabian Shield exhibits an intricate structural framework due to the overprinting effects of multiple Neoproterozoic and Cenozoic tectonic events. This framework includes northeast-trending thrust and reverse faults formed in response to the accretion of multiple Precambrian island arcs, in addition to north-northwest trending normal faults that are associated with the opening of the Red Sea (Camp and Roobol 1989; Stern and Johnson 2010). In particular, the study area is intersected by the Najd Fault System (Fig. 1), a long network of left-lateral strike-slip faults and ductile shear zones that traverse the Arabian Shield and part of Egypt in an NW-SE direction. This fault system is

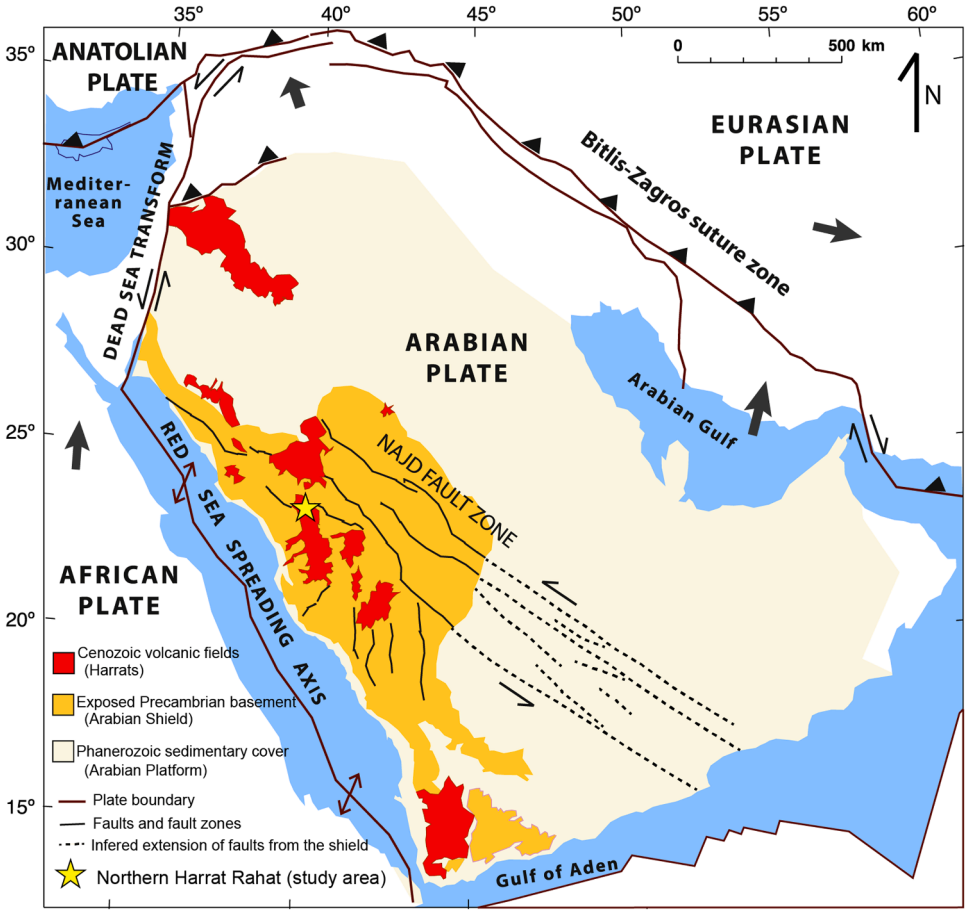

Fig. 1. Plate tectonic and structural setting of the Cenozoic volcanic fields within the Arabian plate (modified from Stern and Johnson 2010 and Langenheim et al. 2018). Dark grey arrows denote plate motions. The yellow star shows the location of the study area.

interpreted to have originated from crustal extension in the northernmost Afro-Arabia region during the Neoproterozoic, thus imprinting a strong structural fabric on rocks of the Arabian Shield (Stern 1985; Camp and Roobol 1989). Cenozoic reactivation of Precambrian faults is also documented, including east-west and north-northwest trending normal faults that extend from the Precambrian basement across and beneath the northern Rahat (Camp and Roobol 1989; Downs et al. 2019). Young faulting within the Rahat is rare or may be concealed beneath younger lava flows, although several northwest-trending fracture systems crosscut some Neogene basalts (Downs et al. 2023). This includes a roughly N30°W large fissure presumably linked with the formation of the Five Fingers lava flows (Roobol et al. 1997).

Geothermal manifestations, such as fumaroles, hot springs, and anomalous high groundwater temperatures, have been observed in association with both post-collisional igneous rocks of the Arabian Shield and Cenozoic volcanic fields. This is because Neoproterozoic-Cambrian post-collisional magmatism has produced peralkaline and peraluminous granitoids enriched in uranium, thorium, and potassium, which could serve as a source of heat through the decay of radiogenic elements (e.g. Chandrasekharam et al. 2016). Conversely, most geothermal manifestations occurring near the Cenozoic volcanic fields are inferred to be linked to the release of gases from magma or associated with geothermal cells beneath the harrats (e.g. Al-Dayle 1980; Lashin et al. 2020).

2.1. *Late Cenozoic magmatism and the formation of the Rahat volcanic field*

Late Cenozoic magmatism throughout the western part of the Arabian Plate resulted in localized igneous intrusions and extensive mafic lava fields, primarily composed of basaltic rocks with minor volumes of more evolved trachytic-rhyolitic lava flows and lava domes, associated with locally preserved pyroclastic successions that form small-volume volcanoes dominated by scoria or spatter cones and subordinate tuff rings (e.g. Camp and Roobol 1989; Downs et al. 2019; Murcia et al. 2016). Arabian volcanic fields older than 10 million years are inferred to be typically more directly linked with the opening of the Red Sea rift, while eruptive products younger than 10 million years have been related to the mantle flow channelized from the Afar Plume along supracrustal dike networks running slightly offset from the Red Sea rift within the Arabian Shield. The Afar Plume is the center of a triple junction that is situated at the intersection of the Red Sea, Gulf of Aden, and East African Rifts (Almond 1986). Particularly, the northward migration of the Afar Plume beneath the Arabian Plate is thought to play a significant role in the distribution of late Cenozoic volcanic fields in western Arabia. This is due to the association of the Afar Plume with the Afro-Arabian Dome, a regionally uplifted area characterized by extensional faulting and fracturing that are inferred to have created pathways for magma (and likely geothermal fluids) migration and ascension through the crust to the surface (Camp and Roobol 1992; Downs et al. 2018).

The Rahat is the most extensive lava field within the Arabian Plate, covering an area of approximately 20,000 km^2 and encompassing >900 observable eruptive vents (Runge et al. 2016; Moufti and Németh 2016). Our study focuses on the northern part of the Harrat Rahat, also known as Harrat Rashid or Harrat Al-Madinah (Fig. 2). The northernmost Rahat mainly comprises small-volume lava flows primarily vented from monogenetic scoria cones that range from alkalic and tholeiitic to hawaiite and mugearite compositions (Murcia et al. 2014; Downs et al. 2018). The predominant basaltic composition of the Rahat magmas is thought to result from the partial melting of garnet peridotite at asthenospheric pressures of 2 to 3 GPa, which is equivalent to crustal depths of around 50–70 km (Al-Mishwat and Nasir 2004). Hypotheses for melt generation include (i) decompression melting associated with the Red Sea spreading center, (ii) asthenosphere upwelling linked to the Afar plume, and (iii) melting of a fossil plume (e.g. Almond 1986; Stein and Hofmann 1992; Camp and Roobol 1992).

2.2. *Rahat volcanic field evolution and morphology*

The northern Rahat is interpreted to have formed through 12 eruptive stages, spanning from the upper Miocene to the present, with a notable northward migration of eruptive centers. The oldest eruptive

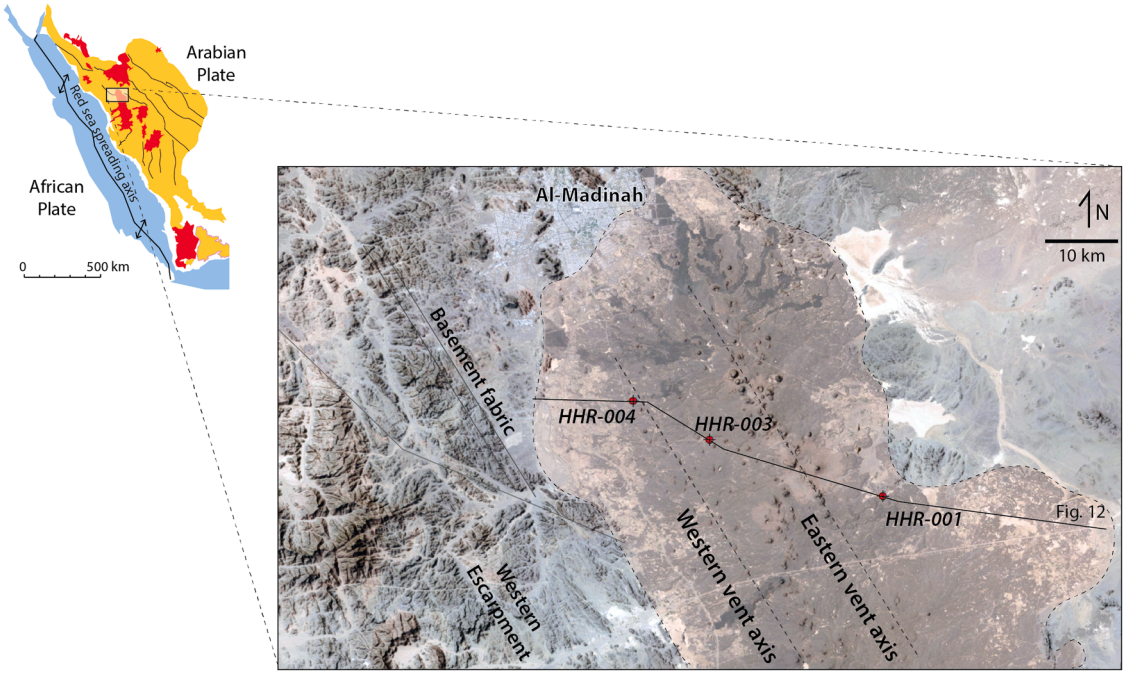

Fig. 2. Structural framework of the northern Rahat volcanic field and its surrounding basement structural trends in relation to the Red Sea spreading center axis. Red polygons mark the distribution of Cenozoic volcanic fields while the orange polygon shows the Precambrian Arabian Shield. The inlet map shows the position of the drillholes perforated in our project and the location of the cross-section presented in the Fig. 12. Satellite image merged with an elevation model from ArcGIS online databank. Dashed black line delimit the polygon corresponding to the outcropping extension of the Harrat Rahat volcanics.

products date back to around 10 million years ago, followed by semi-continuous volcanism from 780 ka to the most recent eruption in CE 1256. Volcanic activity appears to have peaked around 460–360 ka (Stage 9) and 260–125 ka (Stages 5 and 6). Since then, activity has gradually decreased, with minor intensified pulses occurring around 100–70 ka (Stage 4) and 45–11 ka (Stage 2), as summarized by Downs et al. (2019).

The location of eruptive vents within the northern Rahat forms two north-northwest trending alignments (Fig. 2), both oriented (sub)parallel to the Red Sea spreading centre at approximately N30°W (Downs et al. 2018). The primary vent axis (Eastern vent axis) delineates the topographic crest of the volcanic field and serves as the locus of most frequent eruptions, with lava flows extending eastward, westward, and northward. A secondary, more dispersed vent axis lies 7–10 km western from the main vent axis (Camp and Roobol 1989; Downs et al. 2019). These vent alignments suggest a structural control in magma propagation and ascent beneath the Rahat and can provide insights into the presence and orientation of subsurface structures that may define the existence of geothermal resources. This hypothesis is supported by the northwest-trending elongated morphology of some individual spatter cones and fissure vents, which is broadly parallel to structures that transect Cenozoic and Precambrian strata surrounding the Rahat (Camp and Roobol 1989; Downs et al. 2018; Downs et al. 2023).

2.3. Proterozoic-phanerozoic basement of the Rahat volcanic field

Only a few drillholes penetrate the entire lava sequence of the Rahat. As a result, most pre-eruptive information is derived from outcropping rocks near the Rahat, along with interpretations of geophysical data (e.g. Pellaton 1981; Abdelwahed et al. 2016; Langenheim et al. 2018; Bedrosian et al. 2019). The Precambrian basement around the northern Rahat primarily consists of Cryogenian-Ediacaran (meta)volcanosedimentary sequences of the Furayh Group (both east and west), while island arc rocks of the Hijaz terrain are exposed adjacent to and extending north of Al-Madinah. Both units underwent deformation to low greenschist facies during Neoproterozoic accretions and were intruded by late- to post-tectonic Neoproterozoic granitoids (Pellaton 1981; Johnson et al. 2013). Phanerozoic sedimentary rocks are stratigraphically juxtaposed between rocks of the Precambrian Arabian Shield and lavas of the harrats, including Paleozoic sandstones that outcrop approximately 60 km northwest of the study area (Powers et al. 1963; Pellaton 1981). Additionally, an early Cenozoic period of extension-initiated subsidence and the deposition of marine and terrestrial sediments into intracratonic basins along northwest trends across the Arabian Shield (Pellaton 1981; Camp and Roobol 1989). Sedimentary rocks within these basins include Paleogene successions of mudstones, shales, and minor limestones, reported to be preserved beneath the Harrat Hadan basalts and at the village of Dhumariyah, 85 km southeast of Al-Madinah (Powers et al. 1963). Furthermore, a prominent escarpment of the Arabian Shield bounds much of the western limit of the Rahat (Fig. 2). This rugged mountain chain, rising about 2000 m above sea level, extends alongside the northwest-southeast axis of the Red Sea spreading center. Boulder conglomerates originating from these hills mark a sudden increase in intracontinental sedimentation in the Arabian Shield, interpreted as the result of a regional uplift event that took place between the first and second stages of the spreading of the Red Sea during the Miocene (Camp and Roobol 1989).

Interpretation of geophysical data also reveals a northwest structure beneath the northern Rahat. A negative gravity anomaly beneath and extending north of the Rahat forms a northwest-trending depression, with the depocenter located beneath and aligned to the Eastern vent axis. Inversion of the gravity data suggests that this depression is up to 600 m deep and corresponds to low-density rocks (Langenheim et al. 2018). Additionally, magnetotelluric inversion shows a shallow (300–1000 m) bowl-shaped conductive layer interpreted to comprise sediments concealed by the Rahat lavas, or to be related to warm groundwater within and beneath the volcanic section (Bedrosian et al. 2019). Collectively, gravity and magnetotelluric maps indicate an asymmetric depression divided by a ridge. The eastern part of the depression is deeper and lies directly below the eastern vent alignment, whereas the western part is shallower and slightly offset from the western vent alignment (Langenheim et al. 2018). The presence of 13.6 Ma old basalts uplifted 300–400 m above the Rahat lavas indicates that most of the subsidence that forms this depression have likely occurred during the middle to late Miocene, shortly after the onset eruption of the basalts (Pellaton 1981). Alternatively, based on aeromagnetic data, Aboud et al. (2015) inferred that the depression forms a deep graben structure with 1 to 2 km of basin fill.

3. Methods

3.1. Exploration programme and well prognostic

Three drilling locations were chosen to assess the geothermal potential of the northern part of the Rahat volcanic field (Fig. 2). Continuous drill cores were collected from all wells with an average recovery rate exceeding 95 %, and standard wireline logs—including density, gamma, resistivity, and caliper—were recorded and detailed in Arola et al. (2024). The selection process was guided by results from structural analysis and field mapping carried out by SGS and GTK from September 2021 to March 2023 (Fig. 3). Additionally, the interpretation of magnetotelluric and gravimetric data conducted by SGS and USGS from 2015 to 2019 was also taken into consideration, which methods are presented in detail by Langenheim et al. (2018) and Bedrosian et al. (2019). The drilling programme involved the design of vertical stratigraphic wells to reach a target depth of 1000 m at each location. These wells were strategically positioned near the southern boundary of the Najd Fault System with the aim of intersecting zones where fractures and faults could potentially provide higher hydraulic conductivity for geothermal fluids. All wells primarily aimed to test the origin of shallow (<1000 m deep) high-conductivity magnetotelluric anomalies (Fig. 4) and the likelihood of finding relatively shallow conventional convection-dominated geothermal systems. The shape of these anomalies, trending parallel to the Eastern and Western vent axis and main regional basement structures, could indicate the upwelling of hot fluids within northwest-trending faults or the existence of clay caps above geothermal reservoirs. Additionally, Distributed Temperature Sensing (DTS), and thermal conductivity data obtained from all drilling locations served as the foundation for evaluating the heat flow and geothermal gradient of the study area in detail – critical information for assessing the performance of unconventional geothermal systems in the northern part of the Rahat. A further well was initially planned to investigate the magnetotelluric anomaly near the Eastern vent axis's northern end and the historical eruptions (Fig. 4). However, this drilling operation had to be canceled due to project goals shifting. The final positions of the wells were adjusted due to limitations in road access and permit requirements for installing the drill rig.

Based on the gravimetric data, the prognostic of the HHR-C001 predicted to drill into ~100 m of Rahat lavas and then encounter Precambrian basement rocks, which if fractured, could host geothermal reservoirs. Beyond information from magnetotelluric anomalies detected at depths ranging from ~500 to 600 m, the well HHR-C002 aimed for an intersection of NW-SE and NE-SW lineaments delineated on gravimetric maps (Langenheim et al. 2018). These lineaments could represent the intersection of main fault zones and potential pathways for geothermal fluids. However, due to drilling issues, HHR-C002 was abandoned and sidetracked by HHR-C003. The drilling prognosis for this location predicted finding a pile of Cenozoic lavas overlaying Phanerozoic sedimentary strata and Precambrian basement rocks. Gravimetric data suggest that the basement should be encountered at depths ranging from 400 to 600 m. At the HHR-C002 and HHR-C003 locations, potential geothermal reservoirs could include sandstones

Fig. 3. (a) Holocene lavas of the northern Rahat volcanic field displaced by a northwest-trending fracture presumably related to the Five Fingers eruption (Roobol et al. 1997). (b, c, and d) Typical NW-SE and NE-SW structures intersect the Neoproterozoic basement that crop out ~3 km west of the Rahat. The Neoproterozoic basement rocks could serve as a fractured reservoir for geothermal fluids beneath the Rahat.

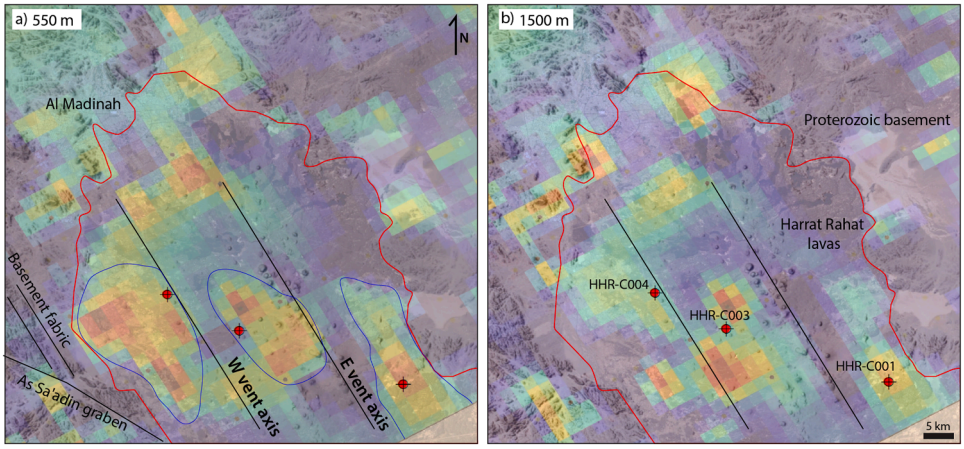

Fig. 4. Magnetotelluric maps showing the geometry of high-conductivity anomalies (hot colors) occurring at (a) 500 m deep and (b) 1500 m deep beneath the northern part of the Rahat and their relationship with the main structural patterns described in the study area. MT maps provided by SGS.

and conglomerate sequences deposited within Phanerozoic intracratonic basins and fractured Precambrian basement rocks. The well HHR-C004 was aimed at the western volcanic vent axis, where a northwest-trending positive magnetotelluric anomaly occurs from approximately 500–1500 m deep. Similar to the HHR-C002 and HHR-C003 wells, potential geothermal reservoirs at this location could form within sandstones and conglomerate sequences deposited within Phanerozoic intracratonic basins as well as fractured Precambrian basement rocks.

3.2. Thermal data

The thermal conductivity of 29 samples was measured under dry conditions at the SGS laboratory using a Hot Disk TPS 2200 instrument employing the Transient Plane Source (TPS) method. This method utilizes a temperature sensor which is sandwiched between two samples to measure the increase in thermal resistance as the sample is submitted to increasing heat through an electrical current pulse (Gustafsson 1991; Heap et al. 2020).

Temperature profiles were measured using fiber optic cables employing the DTS method. DTS cables accurately record continuous temperature data to depths of several kilometers, with a resolution of <1 m between measured points. The method is based on the Raman scattering principle, in which a light pulse is induced into one end of the fiber optic cable and recorded as it travels downhole. As the light pulse travels along the cable, it interacts with the surrounding environment, and temperature changes along the length of the cable cause backscattering of light. This, in turn, affects the speed of light propagation in the

fiber. By measuring the time it takes for backscattered light to return to the instrument, the temperature along the fiber can be estimated. (Farahani and Godolla 1999; Hakala et al. 2021). In this project, DTS data was utilized to deduce the geothermal gradient of the study area. Variations observed in the upper section of the wells were attributed to rock heterogeneity and influence of fluid flow. Therefore, we approach our calculations in two distinct ways: (i) using DTS data over the entire drilled interval, considering all rock units, and (ii) Using data from the basement section alone, where rock heterogeneity and active fluid flow effects are minimized. Our calculated geothermal gradients served as the basis for estimating the deeper geothermal potential of the area (up to 10 km deep), under the assumption that heat transfer occurs solely through conduction in the study area. Variables such as the possible presence of deep faults, the existence of small magma-mush bodies beneath the Rahat, and unknown lithological variations at depths >1 km imply uncertainties that constrain our estimations.

The DTS data, along with the thermal conductivity of the analyzed rocks, were used to calculate the study area's heat flow. This physical property refers to the amount of heat energy transferred through a unit area over a specific time, typically expressed as milliwatts per square meter (mW/m^2), where one watt represents one joule of energy transferred per second. Assuming a conductive-dominated heat transfer, heat flow was determined using the following equation (Incropera et al. 2007):

$$Q = -k \cdot \frac{dT}{dz}$$

where k is the thermal conductivity of the rocks and dT/dz is the measured geothermal gradient over a specific depth interval. Most thermal conductivity data was sourced from our lab measurements of key rock types that occur in the area (Table 1). The thermal conductivity of gravels and sediments not analyzed in our laboratory tests were complemented by data presented in Cermak and Rybach (1982). Here, heat flow was calculated as the average of all rock units encountered at each well location, solely considering data from the basement section (Table 2).

3.3. Hydrogeochemistry

To determine the hydrogeochemical characteristics of the study area, 20 representative samples were collected from depth intervals ranging from 200 to 986 m (Appendix 1). Samples were collected by the Technology Expert Company (TEC), and geochemical tests were performed at the SGS laboratory, except for samples from the well HHR-C001, which were analyzed by TEC. Initially, the groundwater level was determined using an electrical conductivity probe, and any floating oil was removed to prevent contamination. TEC uses a cylindrical metal bailer probe with a diameter of 60 mm, a length of 2.5 m, and a volume capacity of 1500 ml to retrieve the samples. The probe has a chamber with up-and-down lids that allow water to pass through with minimal disturbance. The chamber contains two electronically operated plugs that seal the sample and prevent contamination while pulling it to the surface. After retrieval, the samples were stored in airtight polyethylene bottles and sent for subsequent laboratory analyses. Each sample was placed into three 500 ml bottles: one for anions concentration, not preserved, one for major and trace cations concentration, preserved by adding 2.5 ml of nitric acid, and one for nutrients preserved by adding 2.5 ml of chloroform. The concentration of the major and minor constituents such as Ca, Mg, Na, K, and Total Dissolved Solids (TDS), and 30 trace elements such as Br, B, and SiO_2 were analyzed following SGS and TEC standard laboratory procedures.

Table 1
Thermal conductivity data measured from key rock types at each well location.

Sample	Well	Depth (m)	Rock unit	Rock type	Thermal Conductivity (W/mK)
1	HHR-C001	6	Rahat volcanics	Basalt	1.974
2	HHR-C001	44	Rahat volcanics	Basalt	1.616
3	HHR-C001	69	Rahat volcanics	Basalt	1.426
4	HHR-C001	94	Proterozoic basement	Metasedimentary	2.716
5	HHR-C001	200	Proterozoic basement	Metasedimentary	2.877
6	HHR-C001	406	Proterozoic basement	Metasedimentary	3.306
7	HHR-C001	506	Proterozoic basement	Metasedimentary	2.621
8	HHR-C001	650	Proterozoic basement	Metasedimentary	3.460
9	HHR-C001	963	Proterozoic basement	Metasedimentary	3.237
10	HHR-C003	90	Rahat volcanics	Basalt	1.844
11	HHR-C003	305	Rahat volcanics	Basalt	1.762
12	HHR-C003	416	Cenozoic sediments	Mudstone	2.056
13	HHR-C003	505	Cenozoic sediments	Mudstone	2.080
14	HHR-C003	590	Cenozoic sediments	Mudstone	2.016
15	HHR-C003	731	Proterozoic basement	Metasedimentary	2.060
16	HHR-C003	820	Proterozoic basement	Metasedimentary	2.048
17	HHR-C003	851	Proterozoic basement	Metasedimentary	2.738
18	HHR-C003	890	Proterozoic basement	Metavolcanic	2.069
19	HHR-C004	20	Rahat volcanics	Basalt	1.700
20	HHR-C004	131	Rahat volcanics	Basalt	1.832
21	HHR-C004	208	Rahat volcanics	Basalt	1.652
22	HHR-C004	269	Cenozoic sediments	Mudstone	1.909
23	HHR-C004	294	Cenozoic sediments	Mudstone	2.509
24	HHR-C004	313	Cenozoic sediments	Mudstone	2.314
25	HHR-C004	474	Cenozoic sediments	Mudstone	2.184
26	HHR-C004	491	Cenozoic sediments	Sandstone	2.495
27	HHR-C004	817	Proterozoic basement	Metavolcanic	2.352
28	HHR-C004	880	Proterozoic basement	Metavolcanic	2.853
29	HHR-C004	970	Proterozoic basement	Metavolcanic	3.038

4. Geothermal assessment of the northern Rahat volcanic field

4.1. Structural framework

Faults that penetrate deep into the crust typically assist fluid flow and localize the occurrence of geothermal fluids (e.g. Ledésert et al. 2009; Duwiquet et al. 2021). Our field mapping and lineament interpretation agree with observations from Pellaton (1981) and Downs et al. (2019) that suggest that the volcanic vent axis is set parallel to the main structural fabric of the Precambrian basement, which is mainly exposed in the western part of the northern Rahat (Figs. 2–4). In detail, this

Table 2
Average thermal parameters measured and calculated for each well location.

Well	Thermal conductivity (W/mK)		Geothermal gradient (°C /km)		Heat flow density (mW/m^2)	
	all units	basement	all units	basement	all units	basement
HHR-C001	2.35	3.03	15.7	15.3	37	46
HHR-C003	2.02	2.22	26	22	53	49
HHR-C004	2.25	2.74	25.3	23.6	57	65

basement fabric primarily consists of pervasive fracture corridors N30°W oriented, with subordinate N30°E fractures and minor E-W structures intersecting (meta)volcanosedimentary rocks of the Furayh Group (Fig. 3bcd). Towards the north of the Rahat, where the Precambrian basement comprises rocks of the Hijaz terrain, the major structures trend N40°W, subparallel to the Rahat eruptive vents alignment and the Red Sea spreading center. Additionally, most Cenozoic dikes outcropping in the Al-Baydha region and to the north of the Rahat also follow a northwest trend (Pellaton 1981), which can provide an analogous for the crustal stress regime beneath the northern Rahat (Downs et al. 2018), as observed in similar monogenetic settings elsewhere (Németh and Kereszturi 2015; Barrier et al. 2021). Furthermore, the northwest-trending orientation of the fissure associated with the Five Fingers eruptions (Roobol et al. 1995; Fig. 3a) further supports the structural links between the basement fabric and the crustal stress regime in the northern Rahat region.

4.2. Drilling results

From top to bottom, HHR-C001 penetrated a volcanic unit consisting of 79.15 m of massive, fractured, and vesicular lava flows, followed by 1.7 m of epiclastic material and paleosols (Figs. 2 and 5). The volcanic unit directly overlies massive grey and green (meta)mudstones, cemented sandstones, as well as compacted polymictic breccias and conglomerates. Sedimentary structures are rare or absent while abundant calcite veins and pervasive chloritization is observed (Fig. 5). In addition, some intervals are often fractured and accompanied by the precipitation of calcite, chlorite, milky quartz, and epidote, and occasionally display polyhedral fractures typically interpreted to form as the result of hydraulic brecciation (Fig. 5; Sanchez-Alfaro et al. 2016; Tsukamoto et al. 2020). These more compact and massive formations are identified continuously downhole to the final depth of 990 m.

Fig. 5. Drill core photographs of the well HHR-C001. (a) shows the contact between the Rahat lavas and the Proterozoic basement. (b) Typically, massive metasedimentary (greywacke) rock of the Neoproterozoic basement transected by multiple calcite veins. (c) Massive greywacke with pervasive calcite cementation and polyhedral fracturing typical of hydraulic brecciation. (d) Massive metaconglomerate with pervasive calcite cementation. Both greywacke and metaconglomerate rocks do not show visible porosity. Drill core lengths are one meter for the entire length of the box and a diameter of four cm.

The well HHR-C002 encountered a highly fractured interval at approximately 700 m depth, and due to drilling issues, it was abandoned and sidetracked by HHR-C003. Therefore, only results from HHR-C003 are reported here. HHR-C003 penetrated 355.55 m of massive, fractured, and vesicular lava flow deposits with varying degrees of alteration. This volcanic unit overlaps a ~50 m thick succession of red mud, clastic sands, and poorly sorted, well-rounded, polymictic gravels comprising granitic, metasedimentary, and quartz clasts up to cobble size (Fig. 6). These sediments overlay a 245.55 m thick succession of green and brown mudstones that show frequent planar and cross-bedding structures at the top of the sequence, followed by weekly bedded clean quartz sandstones and minor polymictic conglomerates (Fig. 6). The bedding is horizontal to sub-horizontal at the top of the sequence, indicating that these deposits were not affected by major tectonic events. Conversely, towards the base of the sequence, small displacement faults are often observed in the drillcores, and the bedding becomes more steeply inclined (up to 30°), suggesting some degree of tectonic deformation (Fig. 6). The sedimentary sequence overlays (meta)sedimentary and (meta)volcanic rocks whose stratigraphic boundary was placed at a depth of 651.10 m, based on variations in the gamma-ray logs (Arola et al. 2023). This lower section comprises compact, mostly massive grey and green mudstones, cemented sandstones, and polymictic breccias and conglomerates (Fig. 6). As observed in the well HHR-C001, sedimentary structures are rare or absent, whereas calcite veins and chlorite are abundant, suggesting low-grade metamorphic processes. From approximately 500 m deep and downhole, the drill cores exhibit highly fractured intervals associated with abundant calcite veins, chlorite, epidote, and pink-colored typically Mn-rich minerals like rhodonite-rhodochrosite, a paragenesis often resulting from high-temperature (>300 °C) hydrothermal alteration (Fig. 6; e.g. Nishimoto and Yoshida 2010; Tsukamoto et al. 2020; Weydt et al. 2022). Zones of cataclastic texture and polyhedral fracturing related to chlorite, milky quartz, and precipitation of calcite affect both the lower sedimentary unit and basement strata, suggesting that these rocks have undergone hydraulic brecciation and fault activity related with hydrothermal circulation.

Rocks found in the well HHR-C004 closely correlate with those observed in HHR-C002 and HHR-C003 (Figs. 7 and 8). From the top, the volcanic unit consists of 217.4 m of massive, fractured, and vesicular lava flow deposits that display various degrees of alteration, followed by approximately 7 m of epiclastic material and paleosols. The volcanic rocks overlap a ~30-meter-thick succession of red mud, clastic sands, and poorly sorted, well-rounded, polymictic gravels up to boulder size. These sediments overlie a ~396-meter-thick succession of green and brown mudstones, quartz sandstones, and minor polymictic conglomerates (Figs. 7 and 8). The sedimentary rocks become sandstone-rich and more conglomeratic from 450 m deep and downhole. The bedding is horizontal to sub-horizontal throughout the entire sedimentary succession, indicating that these deposits were not affected by major tectonic events or tilting. From ~670 m deep and downhole, the rocks comprise massive mudstones, cemented sandstones, polymictic breccias, and conglomerates. Similarly to lithological and textural observations from the other wells, rocks in HHR-C004 also display diverse highly fractured intervals, small fault displacements, and evidence of high-temperature

Fig. 6. Drill core photographs of the wells HHR-C002 and HHR-C003. (a and b) Laminated mudstone transected by multiple small displacement faults and veins. (c) common cataclastic texture associated with veining and polyhedral fractures, typical of rocks that have experienced hydraulic brecciation. (d) Cataclastic texture and veining associated with precipitation of rhodonite-rhodochrosite, typical of rocks affected by high-temperature (~300 °C) hydrothermal fluids. (e) Proterozoic basement rock displaying intense cataclastic texture, polyhedral fractures, and transected by multiple calcite and milky quartz veins. Drill core lengths are one meter for the entire length of the box and a diameter of four cm.

hydrothermal activity, including multiple calcite veins, cataclastic zones, and minerals such as chlorite and rhodonite-rhodochrosite infilling cracks (Fig. 8).

4.3. Lithological interpretation

The volcanic unit and paleosols are directly related to lava flows and reworked material originated from the Rahat volcanic field (Figs. 5 and 7). The gravels and red mud (Figs. 6 and 7) could tentatively be correlated to alluvial sediments originating from the regional uplift of the western Arabian shield during the Miocene (Camp and Roobol 1989), whose are here referred to as “alluvial unit”. The underlying sequence of sedimentary rocks (Figs. 6–8) may be attributed to the deposition of marine and terrestrial sediments into intracratonic basins formed across the Arabian Shield (Powers et al. 1963; Camp and Roobol 1989). The precise age of this sedimentary sequence is not yet known, but the concordant stratigraphic relationship with the overlaying alluvial unit suggests Cenozoic deposition, and thus are here informally referred to as “Cenozoic sedimentary unit”. An alternative scenario is that at least part of this sedimentary sequence correlates to Paleozoic sedimentary successions that crop out northwards the Rahat (Pellaton 1981). The massive, compact, (meta)sedimentary sequence is identified as basement rocks of the Furayh Group, which has undergone low-grade metamorphic processes, likely related to the Proterozoic island-arc accretions (Camp and Roobol 1989; Stern and Johnson 2010). However, detailed criteria to distinguish whether Cenozoic conglomerates originate from the erosion of Furayh Group rocks or from in situ arc-collisional strata of Precambrian age are yet to be established. Grey basement rocks with pseudo-vesicular texture are tentatively described as metavolcanic rocks of the Shaqran Formation, a subunit of the Furayh Group.

4.4. Thermal conductivity, temperature profiles, and heat flow

Thermal conductivity values of 29 samples range from 1.43 to 3.46 W/Km. Volcanic rocks exhibit the lowest values, averaging 1.73 W/Km. In contrast, sedimentary rocks have average values of 2.20 W/Km, while basement rocks display the highest thermal conductivity, averaging 2.72 W/Km. Specifically, metavolcanic basement rocks have an average thermal conductivity of 2.58 W/Km, while metasedimentary basement rocks show an average of 2.78 W/Km (Table 1).

Analysis of DTS data over a depth interval up to 1000 m reveals that the average geothermal gradient in the northern Rahat area is approximately 22.3 °C/km when considering all rock units, and 20.3 °C/km based solely on data from the basement section (Fig. 9; Table 2). For each well, the geothermal gradient is consistently lower in the basement section compared to the entire drilled interval, which can reflect the higher thermal conductivity of the basement rocks (Table 2). In detail, the lowest geothermal gradient was recorded in the well HHR-C001, located in a basement high, with a geothermal gradient of 15.3 °C/km over the basement interval. In contrast, wells HHR-C003 and HHR-C004, situated within the depression below the Rahat and thus covered by a ~650 m thick volcanic and sedimentary pile, exhibit much higher basement geothermal gradients of 23 °C/km and 23.6 °C/km, respectively (Figs. 9 and 10). This thermal anomaly could result from the relatively low thermal conductivity properties of the overlying volcanic

Fig. 7. Drillcore photographs of the well HHR-C004. (a) Massive and vesicular lavas of the Rahat. (b) Gravel up to boulder size overlaying sub-horizontal red laminated mudstones presumably of Miocene age. (c) Sub-horizontal laminated mudstones interbedded with very fine-grained sandstone likely deposited during the Cenozoic. (d) Proterozoic basement rocks with pervasive calcite and milky quartz veining. Drill core lengths are one meter for the entire length of the box and a diameter of four cm.

Fig. 8. Drill core photographs of the well HHR-C004. (a and b) Sub-horizontal laminated mudstone transected by multiple calcite and milky quartz veins, and small displacement faults. (c) sub-horizontal laminated mudstones (left) and medium-grained sandstone with pelitic intraclasts. Both rocks are transected by multiple veins and show evidence of small displacement faults. (d) Neoproterozic basement rock displaying polyhedral fractures associated with the precipitation of calcite, chlorite, and milky quartz, typical of rocks that experience hydraulic brecciation and hydrothermal activity. (e) detail of the breccia in (d). Drill core lengths are one meter for the entire length of the box and a diameter of four cm.

and sedimentary sequences, potentially creating a thermal blanket effect in the Rahat area, as proposed to occur in basement settings covered by sedimentary rocks elsewhere (Martinkauppi and Piipponen 2022). Additionally, minor sections, <20 m thick, exhibit a decrease in temperature, likely due to active groundwater flow within permeable zones (Fig. 9).

The average heat flow density of the area was calculated as 37 mW/m^2 at the location of well HHR-C001, 53 mW/m^2 at HHR-C003, and 57 mW/m^2 at HHR-C004, considering DTS and thermal conductivity data from all rock units. Specifically for the basement section, the average heat flow density is 46 mW/m^2 at HHR-C001, 49 mW/m^2 at HHR-C003, and 65 mW/m^2 at HHR-C004. For each well, the heat flow in the basement is higher compared to the results calculated for all rock units at wells HHR-C001 and HHR-C004, but lower at HHR-C003 (Figs. 9 and 10; Table 2). This variation likely reflects the interplay between thermal conductivity and geothermal gradient at each location.

4.5. Fluid geochemistry

Hydrogeochemical analysis indicates that all collected samples fall into the Na-Cl groundwater facies. In detail, the groundwater composition exhibits distinct trends with increasing depth and varying well locations, which are strongly influenced by the presence of fault zones and lithological changes (Fig. 11). Chemical concentrations in HHR-C001, situated on the basement high, differ from other wells situated in the depression where the volcanic and Cenozoic sedimentary unit are deposited. These differences are highlighted by the general downhole increase of Na+ and Cl- ions in HHR-C001, whereas these elements decrease in the other two wells. Similarly, the groundwater salinity, as indicated by the Total Dissolved Solids (TDS), drastically differs from wells. In HHR-C001, TDS levels remain relatively stable down to 100 m above sea level (MASL), after which they exhibit a noticeable increase, rising from 2050 mg/l to 5300 mg/l. Contrarily, samples from wells HHR-C003 and HHR-C004 exhibit an inverse trend, with salinity decreasing from 3500 mg/l to 700 mg/l around the same 100 MASL depth, aligning with the location of fault zones identified in both wells (Fig. 11a). The concentration of SO_4^{2-} and Mg^{2+} ions increase with depths in HHR-C003, while HCO^{3-} and Ca^{2+} are more pronounced in HHR-C004 (Supplementary material).

The distribution of trace elements also exhibits specific trends that vary with depth and the locations of the wells. Br-, B, and also SiO_2 concentrations follow the salinity trend in HHR-C003 and HHR-C004, whereas these components are consistently low or below the analytical level along the HHR-C001 length. Br- and Cl- are relatively conservative groundwater components and their ratios can help distinguish between different water sources. Jahnke et al. (2019) reported rBr/rCl ratio in the Red Sea water ranging from 649 to 714 and from 2500 to 100,000 in various evaporitic environments in the Middle East region. The rBr/rCl ratio for wells HHR-C003 and HHR-C004 resembles this average seawater ratio, with values ranging from 500 and increasing downhole to 800 mg/l from 100 MASL (Fig. 11b). In contrast, HHR-C001 exhibits a notably higher ratio around 1000–4000, which increases dramatically to values above 50,000 at around −100 MASL.

Overall, the hydrogeochemical results indicate diverse sources of groundwater. Specifically, in the well HHR-C001, the composition patterns suggest contact with evaporites during recharge and minimal groundwater circulation. In addition, depth trends imply lower recharge rates for deeper and older groundwater at the time of infiltration, allowing more time for equilibration with evaporites. In wells HHR-C003 and HHR-C004, the groundwater composition indicates a blend of leaching marine porewater, recharged water influenced by evaporite dissolution, and low-salinity groundwater within the basement fault zones. There is no evidence suggesting that these fault zones are linked to a deep heat source, as typical elements found in high-temperature areas, like B and SiO_2 (Arnorsson and Andresdottir 1995; Fournier 1977) exhibit a decrease with increasing depths in HHR-C003 and HHR-C004 (Fig. 11; Supplementary material). Given the necessity to identify end-member components to isolate the effects of water-rock interactions, geothermometry was not attempted within the

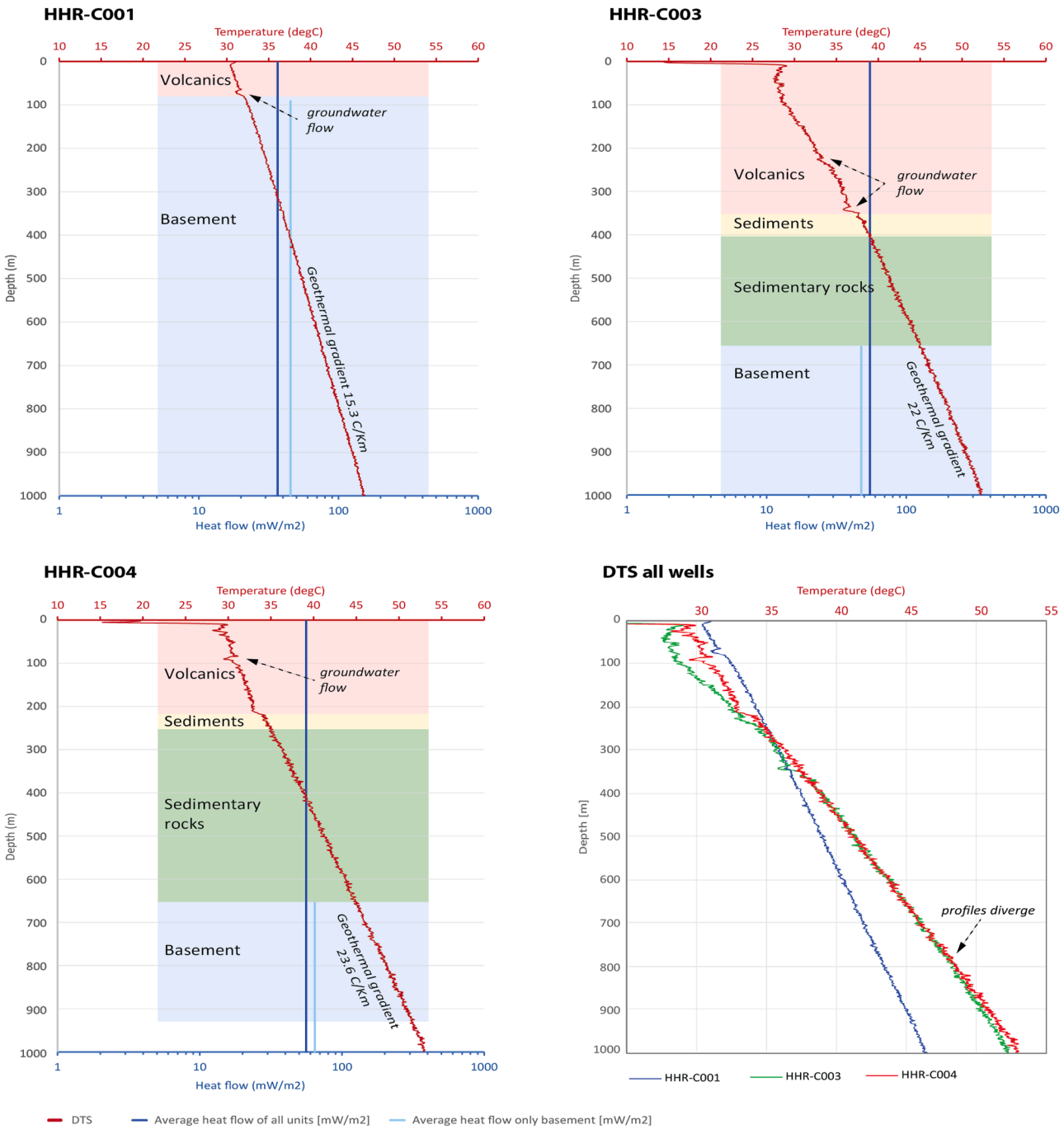

Fig. 9. DTS measurements (red line) and average heat flow (blue lines) as a function of depth for each well. The lowest geothermal gradient of 15.3 °C/km was recorded in well HHR-C001 over the basement interval. Wells HHR-C003 and HHR-C004 exhibit geothermal gradients between 22 °C/km and 23.6 °C/km, respectively, over the basement section.

framework of this paper.

5. Discussion

5.1. Pre-eruptive structure of the northern Rahat volcanic field

The results of our drilling program confirm the existence of a shallow graben concealed by the Rahat lavas (Fig. 12). The well HHR-C001 drilled onto a basement high, outside the eastern boundary of the graben, recovering a thin (~80 m) pile of basalts deposited directly on Precambrian rocks. By contrast, HHR-C003 and HHR-C004 were drilled within the gravity-based graben boundaries. These wells penetrated a much thicker pile of basaltic rocks (over 200 m), followed by a succession of gravels and sedimentary rocks, reaching the Proterozoic basement at a depth of ~600 m, agreeing with geophysical interpretations from Bedrosian et al. (2019) and Langenheim et al. (2018). The base of the basaltic unit was found at an equivalent elevation (from the present sea level) in both the HHR-C003 and HHR-C004 wells, suggesting that the Rahat lavas infilled a relatively flat and shallow topographic depression (Fig. 12). This interpretation is reinforced by the nearly continuous thickness of the alluvial unit across both wells, indicating that most of the subsidence that accommodated the depression occurred before the deposition of the alluvial unit, presumably in the Miocene, and consistent with Pellaton's (1981) interpretation.

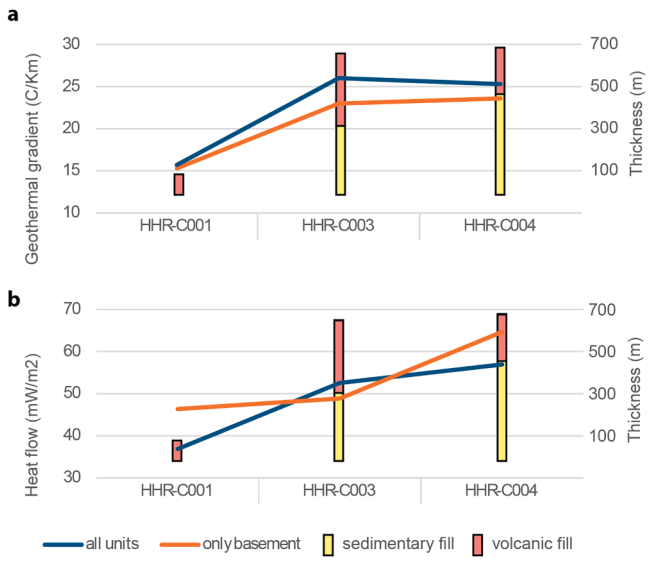

Fig. 10. Geothermal gradient and heat flow calculated for each well location and their relationship with the basin fill thickness.

Assuming little lateral variation across the graben, it is evident that the volcanic pile is much thicker beneath the eastern vent alignment, in agreement with observations from gravity inversion (Langenheim et al. 2018). Our drilling results confirm that the maximum thickness of the volcanic pile is around 600 m at the eastern vent alignment, also supporting Pellaton's (1981) estimations. The 2D geometry of this depression is represented in Fig. 12, more closely resembling a bow-like depression (Langenheim et al. 2018; Bedrosian et al. 2019) rather than a prominent basement structure bounded by large offset (>1 km) normal faults (Aboud et al. 2015). Conversely, the tilting and dominance of sandstones and conglomerates within the lower part of the sedimentary sequence indicate some degree of tectonic activity concurrently with the early stages of the depression formation. This suggests that large offset faults or fault zones with displacements of up to 500 m may exist, particularly at the eastern and western boundaries of the depression (Fig. 12). These faults may constitute important targets for further geothermal exploration in the area. A seismic reflection profile across the northern Rahat would be greatly valuable in determining the location and geometry of these faults.

5.2. Geothermal reservoirs

No active geothermal reservoirs were identified through drilling, although porous and fractured rocks were encountered in all wells. The volcanic unit comprises abundant intervals of fractured-vesicular basalts commonly interpreted to exhibit good reservoir properties (e.g. Holford et al. 2021; Bischoff et al. 2021; Rossetti et al. 2022; Millett et al. 2023). Similarly, the alluvial unit immediately concealed by the Rahat lavas could constitute a reservoir target (Fig. 7). However, these units are unlikely to contain high-enthalpy fluids, which are expected to migrate through fractures within the Rahat basalts and manifest at the surface as fumaroles. Alternatively, a self-sealing process such as the formation of clay caps above the reservoir could explain the lack of geothermal manifestations. Nevertheless, no evidence of clay caps was found in the drill cores. Additionally, DTS data only record relatively low-temperature (<35 °C) groundwater flowing within these units (Fig. 9), which opposes the occurrence of high-enthalpy geothermal fluids. Most likely, the shallow conductive layers observed in the magnetotelluric data represent mudstone rocks concealed beneath the Rahat lavas, as previously suggested as a possible explanation by Bedrosian et al. (2019), rather than form clay caps above geothermal reservoirs. Although unlikely, we cannot disregard that these units may host geothermal fluids in other areas not yet assessed by drilling.

The Cenozoic sedimentary unit mainly comprises fine-grained sequences that exhibit low reservoir potential. The absence of hydrothermal manifestations on the Rahat volcanic field may be attributed to these fine-grained sedimentary rocks sealing deeper geothermal reservoirs, although we did not find evidences supporting this interpretation. This sequence becomes progressively sandstone-rich towards the base and includes minor conglomerate packages that are likely to present substantial porosity and permeability. Additionally, this unit is often intersected by multiple fractures and faults that could increase its hydraulic conductivity (Figs. 6–8).

The metasedimentary basement rocks of the Furayh Group are typically massive, characterized by pervasive calcite and chlorite cementation, and are thus unlikely to preserve primary porosity. However, observations from both outcrops and boreholes indicate that these rocks often exhibit sets of closed-spacing open fractures that can serve as potential geothermal reservoirs (Figs. 3 and 5). The distinctive geochemical composition observed in the lower sections of wells HHR-C003 and HHR-C004 (Fig. 11) supports the interpretation of active groundwater flow within faults in the study area, although the low SiO_2 and B concentrations do not indicate connection high-a temperature geothermal source. Basement structures within the Precambrian basement beneath the northern Rahat likely control magma ascent (Pellaton 1981; Downs et al. 2018) and could potentially indicate the presence of geothermal fluids not found during our drilling program.

5.3. Conventional geothermal systems

All three boreholes exhibit a modest geothermal gradient of up to 23.6 °C/km, characterized by a typical conductive-dominated profile, where the temperature gradually increases with depth (Fig. 9). This figure aligns with the usual low geothermal gradient observed in crystalline shield areas. Similarly, the low heat flow (up to 65 mW/m^2) values are typical of cratonic areas, contrasting sharply from active geothermal zones, which often exhibit heat flow exceeding 100 mW/m^2 (e.g. Flóvenz and Saemundsson 1993; Lucazeau 2019; Jolie et al. 2021).

Although the DTS data did not record active geothermal systems, the combined mineralogical and textural evidence indicates that relatively shallow, high-enthalpy geothermal fluids likely existed in the Rahat area in the past (Figs. 6 and 7). The mineral paragenesis including chlorite, epidote, and rhodonite-rhodochrosite is interpreted to result from hydrothermal events with temperatures reaching nearly 300 °C (Nishimoto and Yoshida 2010; Tsukamoto et al. 2020; Weydt et al. 2022). In addition, we noted these minerals associated with fractures, faults, and zones of cataclastic texture that suggest hydraulic brecciation mechanisms (Sanchez-Alfaro et al. 2016; Bischoff et al. 2024). As no evidence of magmatic intrusions or peperites was found, we choose to attribute the genesis of these minerals to hydrothermal activity rather than linking them to contact metamorphism associated with rising magma and skarn formation. We observe that this high-temperature mineral paragenesis has affected the sedimentary succession situated directly beneath the alluvial unit, potentially occurring at depths shallower than 1000 m.

The low heat flow of the area and modest geothermal gradient measured in all boreholes argue against the existence of a sizable, long-lived magma chamber emplaced within shallow (<15 km) levels of the crust beneath the northern Rahat. This is also consistent with the general monogenetic nature of the surface manifestation of volcanism in the region (Németh and Kereszturi 2015), further reinforced by the relative primitive composition of the Rahat eruptions, indicating little crustal assimilation (Downs et al. 2018), and by geophysical surveys pointing to a deep (>50 km) source of melt (Bedrosian et al. 2019). However, the presence of shallow small magma bodies cannot be ruled out as some more evolved volcanic rocks are known from the northern Rahat even in the Holocene (Stelten et al. 2020; Stelten et al. 2023; Downs et al. 2023).

Even though our drilling programme did not identify active hydrothermal systems, as the targeted high-conductivity magnetotelluric

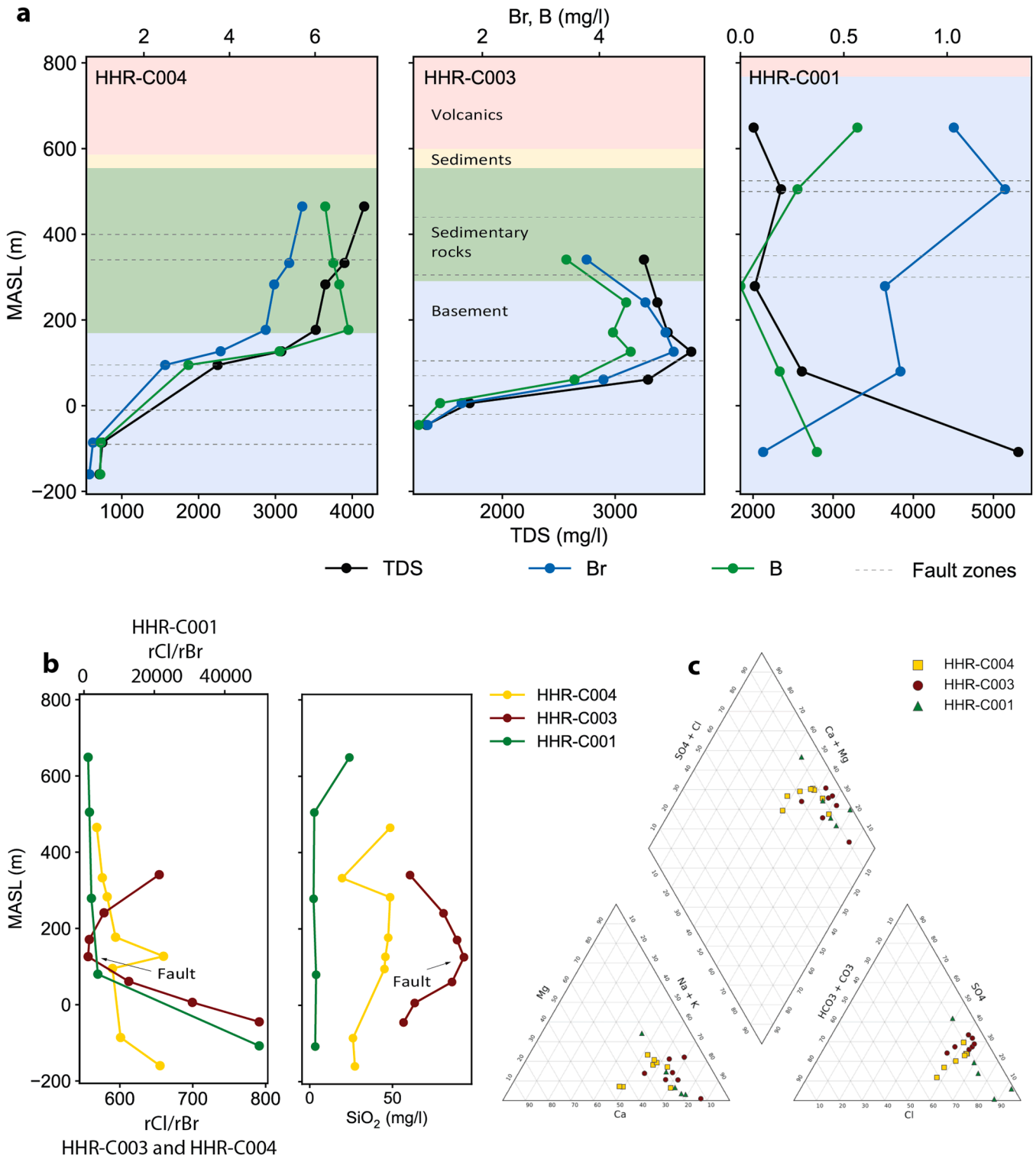

Fig. 11. Groundwater composition parameters and their relation to geological and structural patterns. (a) TDS, Br, B concentration evolution with depth. (b) rCl/rBr and SiO_2 concentration in groundwater. (c) Piper`s diagram shows the predominance of sodium-chlorine groundwater facies.

anomalies more likely result from fine-grained sedimentary rocks, three hypothetical geothermal plays could guide future exploration in the area (Fig. 13). Play #1 consists of a heat source provided by a yet unidentified convective geothermal cell associated with fractured basement reservoirs and confined below Cenozoic fine-grained sedimentary rocks and/or clay caps. The likelihood of this play is moderate, based on the relationship between basement faults and the Rahat eruptive centers, which suggests that geothermal fluids may follow these structures. This play is supported by thermal anomalies recorded in legacy boreholes and historical fumaroles, suggesting that hotter fluids could be confined within narrow fractured reservoir zones (Roobol et al. 1995; Aboud et al. 2022). Play #2 comprises small and shallow intrusions (<5 km deep) that feed heat into fractured basement reservoirs concealed by clay caps. The likelihood of this play is moderated to low because it's uncertain whether shallow intrusions of substantial size (>1 km^3) have been emplaced beneath the Rahat within the last thousand to tens of

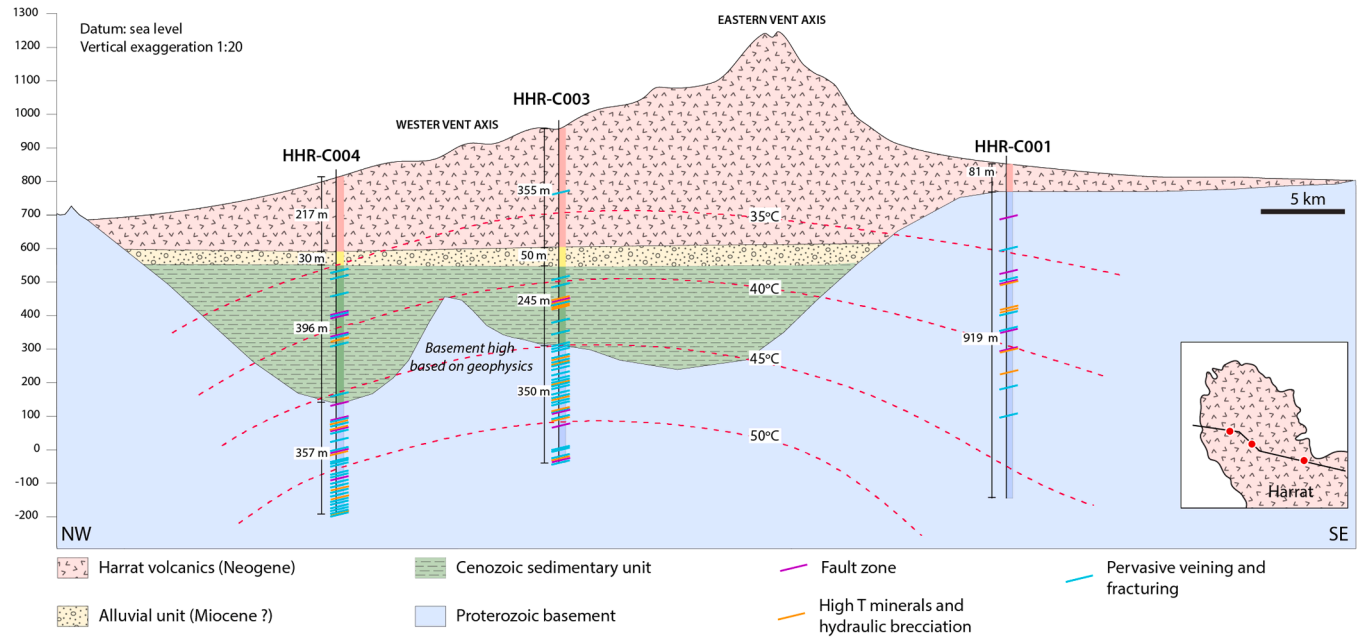

Fig. 12. Cross-section across the northern Rahat showing the location of the main stratigraphy units, geothermal contours, structures, and occurrence of minerals typically related to high-temperature hydrothermal fluids. The section does not account for large fault displacement, piercing of igneous intrusions, or substantial lateral lithological variations within the stratigraphic units. Red dashed lines show geothermal contours estimated from a conductive-dominate profile based on the measured DTS data from each well perforated during our research programme. The geometry of the basement is based on the drilling results combined with gravimetric interpretation from Langenheim et al. 2018.

thousands of years. Play #3 consists of a convective heat source linked to coarse-grained Cenozoic sedimentary rocks concealed by clay caps or fine-grained Cenozoic sedimentary rocks. The likelihood of this play is low because our DTS measurements did not show positive thermal anomalies related to rocks deposited within the graben.

5.4. Unconventional geothermal systems

While conventional systems rely on naturally occurring geothermal reservoirs typically found at depths <4 km, unconventional systems often tap deeper into low-permeability rock formations to harness geothermal power. These innovative approaches and technologies, such as Enhanced Geothermal Systems (EGS) and Advanced Closed Loop (ACL), use techniques like hydraulic stimulation to create artificial reservoirs or employ multilateral wells design to expand the accessibility of geothermal resources (e.g. Brown et al. 1999; Breede et al. 2013; Kraal et al. 2021). Diverse thermogeological and engineering parameters, including (i) the geothermal gradient of the area, (ii) thermal conductivity of surrounding rocks, (iii) enhanced hydraulic connectivity, (iv) reservoir volume, (v) achieved working temperatures, and (vi) the fluid flow rate at which the system operates, play critical roles in determining the final yield of unconventional geothermal technologies (e.g. Kelkar et al. 2016; Jolie et al. 2021; Khodayar and Björnsson 2024). Since many of these technologies are still under development, assessing the potential of unconventional geothermal resources involves several uncertainties, which impose constraints on our resource estimations. To address these limitations and offer a first-order assessment of possible unconventional geothermal systems in the Rahat area, we compare our thermogeological data with the performance of both experimental and commercial EGS and AGS projects documented in the literature (Fig. 14).

Overall, after a reservoir is engineered with a bottom hole temperature ranging from 170 to 200 °C, the expected capacity of doublet EGS systems typically ranges between 1 and 5 MWe and 5 to 30 MWth. These figures align with the performance of several EGS cases, including (i) Fenton Hill in California, where reservoir temperatures of approximately 170 °C and flow rates ranging from 5 to 18 L/s resulted in a capacity of 3–10 MWth (Kelkar et al. 2016); (ii) Fervo Project Red in Nevada, which achieved a capacity of 3.5 MWe during a production test from a reservoir with temperatures of 186 °C and a flow rate of 63 L/s (Norbeck and Latimer 2023); and (iii) Soultz-sous-Forêts and Rittershoffen geothermal plants in France, which have an installed gross capacity of 1.7 MWe and 24 MWth, respectively, utilizing reservoirs with temperatures close to 170 °C (Genter et al. 2010; Frey et al. 2022).

In a best-case scenario where the volcanic pile is thicker and the geothermal gradient is higher (Fig. 12), our thermal data suggests that temperatures close to 170 °C can be reached at depths of approximately 6 km, assuming solely a gradual conductive heat transfer mechanism (Fig. 14). At these depths, the combination of elevated lithostatic pressure and the typical elastic behavior of mechanically induced fractures presents challenges for constructing EGSs capable of sustaining substantial hydraulic conductivity. This is exemplified by the Otaniemi-St1 project in Finland, which successfully connected two wells in a crystalline setting at a maximum depth of 6.4 km. Permeabilities in the order of 10^{-15} m^2 were achieved during a pumping test with flow rates ranging from 6.7 to 13.3 L/s at 60–90 MPa injection pressure. However, upon releasing the well-head pressure, the permeability dropped to pre-stimulation conditions of around 10^{-18} m^2, and the project was terminated in 2022 (Kukkonen et al. 2023). Conversely, one of the world's deepest commercial EGS projects is currently under construction in the United Downs, UK. This project has successfully connected two wells drilled into a fault zone at a maximum TVD of 5058 m, achieving flow rates of up to 60 L/s during hydraulic stimulation (Reinecker et al. 2021). The United Downs EGS system is anticipated to commence operation still in 2024, with a forecasted contribution of 2–3 MWe to the local electricity grid. Additionally, this geosystem has also discovered world-class lithium concentrations in the geothermal brine (Farndale and Law 2022).

Additional unconventional geothermal solutions could be investigated for the northern Rahat area (Fig. 14). For instance, multilateral doublet ACL systems are currently being under development in sedimentary and crystalline settings (Khodayar and Björnsson 2024). While

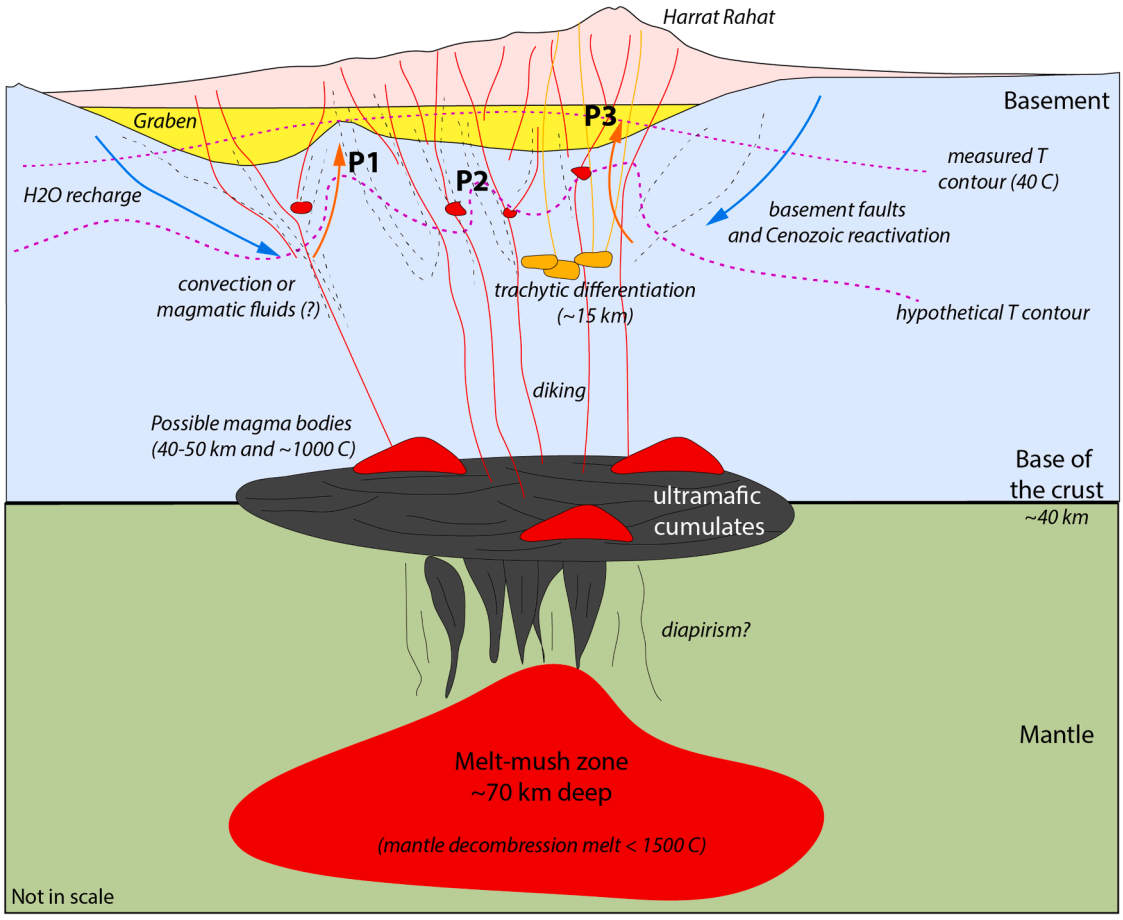

Play 1
Source: convective cells
Migration: faults
Reservoir: fractured basement
Cap: Cenozoic sediments; clay-caps
Likelihood: moderated

Play 2
Source: small shallow intrusions
Migration: fractures; conduction
Reservoir: fractured basement
Cap: clay-caps
Likelihood: moderated-low

Play 3
Source: convective cells
Migration: faults
Reservoir: Cenozoic sediments
Cap: clay-caps; Cenozoic sediments
Likelihood: low

Fig. 13. Hypothetical conventional geothermal plays in the northern part of the Rahat volcanic field. Information compiled from Bedrosian et al. (2019), Downs et al. (2019), and the new insights from our exploration project.

no ground-true data yet exist about the performance of these systems in basement rocks, a similar demonstration plant has been operating since 2019 in a sedimentary setting in Alberta, Canada. Results from the Alberta site indicate positive outcomes, including the effectiveness of casing technology in preventing leakage to the formation, closed-loop flow rate of 9.7 L/s without the need for pumping, and the ability to offer adjustable dispatchability according to demands (Zatonski and Brown 2023). However, challenges persist in closed-loop geothermal technology, particularly regarding the low coefficient of heat transfer in conduction-dominated systems (Toews and Holmes 2021; Beckers et al. 2022; Piipponen et al. 2022) and the high drilling costs associated with multilateral wells extending many tens of kilometers. Additionally, numerical modeling suggests that at depths of 3 km, single-well coaxial ACL systems have a capacity of approximately 200 kWth in relatively low-temperature, impermeable crystalline conditions (Piipponen et al. 2022). At 3 km deep, temperatures are estimated to be around 90 °C in the study area (Fig. 14), posing a challenge for electricity generation at an industry-relevant scale. For these lower temperatures ranging from 80 °C to 100 °C, emerging technologies such as Hybrid Geothermal Systems (HGS) utilize a single coaxial tube-in-tube well connected to an EGS reservoir at depth (Fig. 14). While limited data exists about the performance of these systems, their forecasted capacity is expected to achieve <1 MWe and <5 MWth in low-temperature settings (Khodayar and Björnsson 2024). Furthermore, shallow geothermal heat pumps and Aquifer Thermal Energy Systems (ATES) constructed at depths <500 m could provide continuous direct heating and cooling power, ranging from 10 to around 2000 kW, respectively (Arola et al. 2014; Korhonen et al. 2024).

5.5. *Further research and considerations*

To build upon the findings of this study and improve the understanding of geothermal potential in the Rahat volcanic field, acquiring detailed seismic reflection profiles, particularly across the northwest-trending direction of both the eastern and western vent alignments, will provide more accurate data on subsurface fault structures and potential magmatic conduits. This seismic data could help define the geothermal plays described in Section 5.3 more precisely, assisting in locating new well sites for future drilling campaigns. Recognizing the extension and geometry of the fault zones in detail will also benefit the development of Enhanced and Advanced geothermal systems helping to identify highly permeable zones or prevent drilling issues related to well instability. Although our drilling data did not find active geothermal reservoirs, further exploration of conventional geothermal systems in the Rahat is justified by the high resource capacity of active hydrothermal systems, typically averaging around 3 MWe to 25 MWe per well

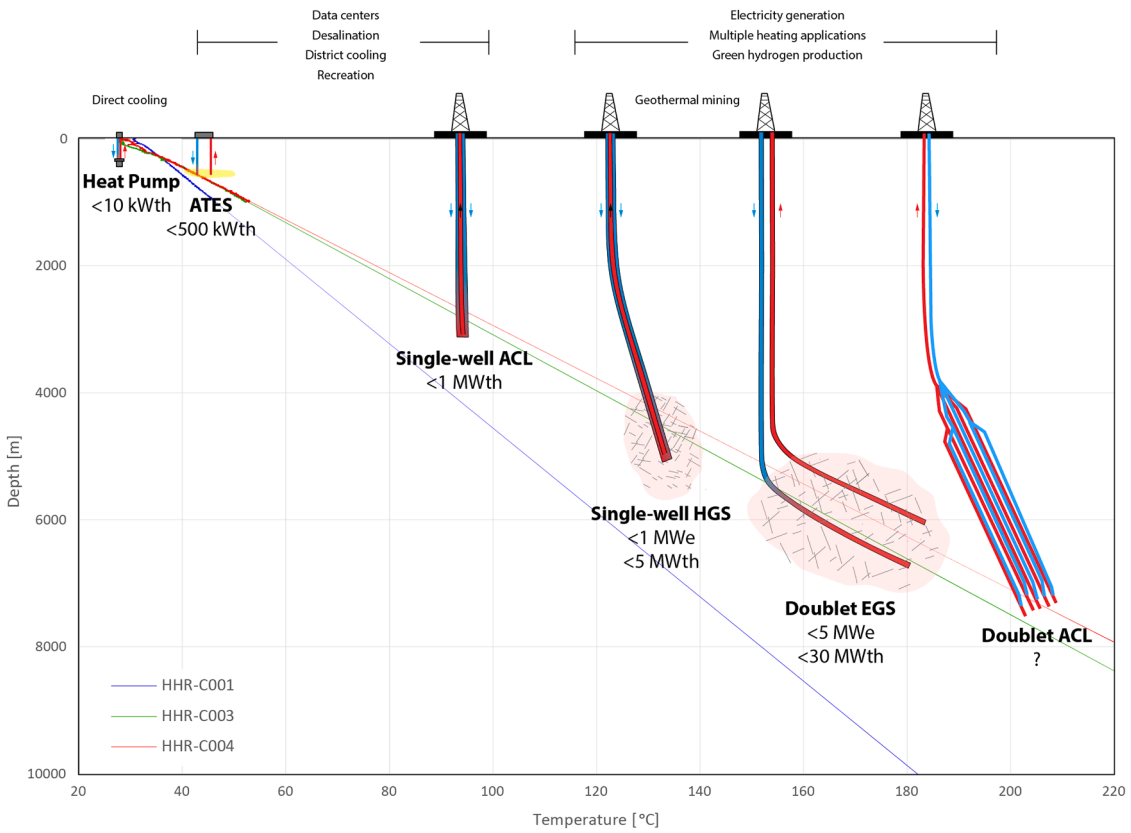

Fig. 14. Estimated depth and potential applications of diverse unconventional geothermal systems in the northern Rahat area. Red, green, and blue lines show the estimated temperature as a function of depth for each well location, assuming a conduction-dominated heat transfer mechanism. The geothermal power capacity is based on data from the literature and is not calculated specifically for the study area.

but potentially reaching as high as 30 MWe to over 75 MWe at modest depths of around 4 km (e.g. Jolie et al. 2021; Dumas et al. 2023).

Additionally, the interpretation of magnetic data should be used carefully to account for potential fossil geothermal systems. Low magnetic anomalies, often linked to the demagnetization of ferromagnetic minerals, may indicate areas of past geothermal activity, rather than operating systems. Furthermore, the age of the stratigraphic units, along with the dating of the identified hydrothermal events, requires further refinement and validation. Future research should focus on developing a comprehensive framework to better understand the evolution and distribution of geothermal fluids in the Rahat area. This framework could focus on determining the age of the fossil geothermal systems, their spatial distribution, and their correlation with the eruptive stages of Rahat. Proving a Neogene age for this hydrothermal event will confirm that shallow (<1000 m deep) high-enthalpy geothermal systems have formed concurrently with the Rahat magmatism.

6. Conclusions

Our exploration programme has yielded valuable insights into the geothermal potential of the northern Rahat volcanic field. Analysis of drilling and field data enabled us to identify crucial geological, structural, volcanological, thermal, and hydrogeochemical characteristics influencing both conventional and unconventional geothermal opportunities in the area. Our drilling results reveal that the maximum thickness of the Rahat volcanic pile reaches approximately 600 m along the eastern vent alignment, confirming the presence of a shallow graben concealed beneath the Rahat lavas. Drilling found that the base of the basaltic unit lies at a consistent elevation in both wells, suggesting that the Rahat lavas filled a relatively flat depression. The consistent thickness of the alluvial unit beneath the volcanic pile indicates that most graben subsidence occurred before its deposition, presumably during the Miocene. Hydrogeochemical data indicate sodium-chlorine groundwater facies with distinctive characteristics influenced by the presence of faults and lithological variations. The distinctive geochemical composition observed within fault zones suggests active groundwater flow in the basement unit; however, the relatively low concentrations of SiO_2 and B at increasing depths do not indicate a high-temperature geothermal connection. Analysis of DTS data reveals a modest geothermal gradient averaging 20.3 °C/km. The lowest values of 15.3 °C/km were found on a basement high, while values of up to 23.6 °C/km were recorded within the graben boundaries. The causes of this anomaly within the graben boundaries may include a thermal blanket effect, attributed to the relatively lower thermal conductivity of the overlying volcanic rocks. Overall, our thermal parameters suggest that heat transfer is primarily governed by conduction rather than convection in the northern Rahat volcanic field. However, several fault zones were found transecting the drillcores which could potentially act as conduits for geothermal fluid migration. Many of these faults are associated with mineral paragenesis and rock textures indicating a fossil high-temperature (nearly 300 °C) hydrothermal event affecting the sedimentary succession beneath the volcanic pile. Confirming a Neogene age for this hydrothermal event would validate the coexistence of shallow conventional geothermal systems with the magmatic evolution of the Rahat area. The relatively low heat flow and modest geothermal gradient measured from all wells argue against the existence of a sizable, long-lived magma chamber emplaced within shallow (<15 km) levels of the crust, although small magma bodies cannot be ruled out. The potential of unconventional geothermal systems in the northern Rahat area presents both challenges and opportunities for energy development. While temperatures of around 170 °C may be reached at depths of approximately 6 km (only considering a gradual geothermal

gradient), the high lithostatic pressure and limited permeability at these depths pose significant constraints on the feasibility of EGSs. Alternative geothermal solutions, such as ACL systems and hybrid geothermal technologies, could offer more practical approaches for energy extraction. Additionally, shallow geothermal systems, including ATES and heat pumps, may provide efficient direct heating and cooling applications. Further research is essential to optimize these technologies and assess their economic viability in the region. By elucidating the volcanological and structural characteristics of the northern Rahat volcanic field and offering insights into its geothermal potential, our research will support future exploration and development of geothermal resources in the Kingdom of Saudi Arabia and similar geological settings globally.

Data availability

The raw data presented in this paper belongs to the Saudi Geological Survey and the Ministry of Industry and Mineral Resources of the Kingdom of Saudi Arabia. Availability will be considered upon request.

Declaration of generative AI and AI-assisted technologies in the writing process

During the preparation of this work, the author(s) utilized ChatGPT and Gemine for grammar review and assistance. After employing these tools, the author(s) thoroughly reviewed and edited the content as necessary and takes full responsibility for the final content of the publication.

CRediT authorship contribution statement

Alan Bischoff: Writing – review & editing, Writing – original draft, Visualization, Validation, Supervision, Methodology, Investigation, Formal analysis, Data curation, Conceptualization. **Khalid A. Bankher:** Writing – review & editing, Validation, Supervision, Project administration, Methodology, Investigation, Funding acquisition, Data curation, Conceptualization. **Ehab A. Alashi:** Writing – review & editing, Validation, Supervision, Project administration, Funding acquisition, Conceptualization. **Teppo Arola:** Writing – review & editing, Validation, Supervision, Project administration, Methodology, Investigation, Formal analysis, Data curation, Conceptualization. **Haitham S. Brinji:** Writing – review & editing, Validation, Resources, Methodology, Investigation, Data curation. **Károly Németh:** Writing – review & editing, Supervision, Methodology, Investigation, Formal analysis. **Annu Martinkauppi:** Writing – review & editing, Validation, Methodology, Investigation, Formal analysis, Data curation, Conceptualization. **Akram H. Jabrte:** Writing – review & editing, Resources, Methodology, Data curation. **Evgenii Kortunov:** Writing – review & editing, Validation, Methodology, Investigation, Formal analysis. **Ibrahim S. Alzahrani:** Writing – review & editing, Validation, Methodology, Formal analysis, Data curation. **Ilkka Martinkauppi:** Writing – review & editing, Investigation, Data curation. **Rami A. Melibari:** Writing – review & editing, Data curation.

Declaration of competing interest

The authors declare that they have no known competing financial interests or personal relationships that could have appeared to influence the work reported in this paper.

Funding sources

This project was funded by the National Industrial Development and Logistics Program (NIDLP), whose main aim is to support the Kingdom's Vision 2030 projects (#UIC: 1–18–065–1379).

Acknowledgments

The authors express their gratitude to Eng. Abdullah M. Al-Shamrani, CEO of the Saudi Geological Survey, for his crucial and ongoing support, which has enabled the project to meet its objectives within the designated timeframe. Special thanks go to geologist Ahmed A. Alashi and geophysicist Naif S. Al-Juaid, both members of the support team, for their invaluable assistance during field activities and data collection. The SGS geophysical team is also acknowledged for their acquiring and processing geophysical data. We appreciate the True East Mining Company (contract no 2022/27) for their efforts to achieve the objectives of the drilling campaign. Finally, we extend our thanks to the SGS Scientific committee and the reviewers of the manuscript for their insightful suggestions to improve the quality of this article.

Supplementary materials

Supplementary material associated with this article can be found, in the online version, at doi:10.1016/j.geothermics.2025.103272.

References

Abdelwahed M.F., El-Masry Nabil, Moufti M.R., Kenedi C.L., Zhao D., Zahran N., Shawali J. 2016. Imaging of magma intrusions beneath Harrat Al-Madinah in Saudi Arabia. 10.1016/j.jseaes.2016.01.023.

Aboud, E., El-Masry, N., Qaddah, A., Alqahtani, F., Moufti, M.R.H., 2015. Magnetic and gravity data analysis of Rahat volcanic field, El-Madinah city, Saudi Arabia. NRIAG J. Astron. Geophys. 4, 154–162.

Aboud, E., Alqahtani, F., Elmasry, N., Abdulfarraj, M., Osman, H., 2022. Geothermal anomaly detection using potential Field geophysical data in Rahat Volcanic Field, Madinah, Saudi Arabia. J. Geol. Geophys. 11, 1026.

Al-Mishwat A.T. and Nasir S.J. 2004. Composition of the lower crust of the Arabian Plate - A xenolith perspective. doi:10.1016/j.lithos.2003.08.003.

Almond D.C. 1986. The relation of mesozoic-cainozoic volcanism to tectonics in the Afro-Arabian dome. 10.1016/0377-0273(86)90024-7.

Arnórsson, S., Andrésdóttir, A., 1995. Processes controlling the distribution of boron and chlorine in natural waters in Iceland. Geochim. Cosmochim. Acta 59, 4125–4146. https://doi.org/10.1016/0016-7037(95)00278-8.

Arola T. Bischoff A. Martinkauppi A. Hietava J. Lahti I. Martinkauppi I. Kortunov E. Wiberg M. 2023. Exploration and evaluation of geothermal energy resources in Al Madinah Al Munawarrah Region. Saudi Geological Survey. Confidential Report, 126p.

Barrier, A., Bischoff, A.P., Nicol, A., Browne, G.H., Bassett, K, 2021. Relationships between volcanism and plate tectonics: a case-study from the Canterbury Basin, New Zealand. Mar. Geol. 433. https://doi.org/10.1016/j.margeo.2020.106397.

Beckers et al. 2022. Techno-economic performance of closed-loop geothermal systems for heat production and electricity generation. 10.1016/j.geothermics.2021.102318.

Bedrosian P.A., Peacock J.R., Dhary M., Sharif A., Feucht D.W., Zahran H. 2019. Crustal magmatism and anisotropy beneath the Arabian shield - a cautionary tale. 10.1029/2019JB017903.

Bischoff, A., Heap, M.J., Mikkola, P., Kuva, J., Reuschlé, T., Jolis, E.M., et al., 2024. Hydrothermally altered shear zones: a new reservoir play for the expansion of deep geothermal exploration in crystalline settings. Geothermics 118, 102895. https://doi.org/10.1016/j.geothermics.2023.102895.

Bischoff, A.P., Fensom, J., Tang, H., Rosetti, M., Nicol, A., 2021. Processes controlling volcanic and epiclastic reservoir formation in a buried polygenetic stratocone. DiCapua, A. (Ed.). Volcanic Processes in the Sedimentary Record: When Volcanoes Meet the Environment. The Geological Society Special Publications. https://doi.org/10.1144/SP520-2021-137. SP520.

Brown, D., DuTeaux, R., Kruger, P., et al., 1999. Fluid circulation and heat extraction from engineered geothermal reservoirs. Geothermics 28, 553–572. https://doi.org/10.1016/S0375-6505(99)00028-0.

Bosworth, W., 2015. Geological Evolution of the Red Sea: historical background, review, and synthesis. N. M. A. Rasul & I. C. F. Stewart (Eds.). The Red Sea: The Formation, Morphology, Oceanography and Environment of a Young Ocean Basin. Springer, Berlin Heidelberg, pp. 45–78. https://doi.org/10.1007/978-3-662-45201-1_3.

Breede, K., Dzebisashvili, K., Liu, X., Falcone, G., 2013. A systematic review of enhanced (or engineered) geothermal systems: past, present and future. Geotherm. Energy 1, 4. https://doi.org/10.1186/2195-9706-1-4, 2013.

Camp V.E. and Roobol M.J. 1989. The Arabian continental alkali basalt province - part I. Evolution of Harrat Rahat, Kingdom of Saudi Arabia. 10.1130/0016-7606(1989)101<0071:TACABP>2.3.CO;2.

Camp V.E. and Roobol M.J. 1992. Upwelling asthenosphere beneath western Arabia and its regional implication. 10.1029/92JB00943.

Cermak, V., Rybach, L., 1982. Thermal properties: thermal conductivity and specific heat of minerals and rocks. G. Angeneister (Ed.). Landolt-B''rnstein Zahlenwerte and Funktionen aus Naturwissenschaften und Technik, Neue Serie, Physikalische Eigenschaften Der Gesteine. Springer Verlag, Berlin, Heidelberg and New York, pp. 305–343. V/1a.

Chandrasekharam D., Lashin A., Al Arifi N., Al-Bassam A.M. 2016. Red Sea geothermal provinces. 10.1201/b20408.
Downs D.T., Stelten M.E., Champion D.E., Dietterich H.R., Nawab Z., Zahran H., Hassan K., Shawali J. 2018. Volcanic history of the northernmost part of the Harrat Rahat volcanic field, Saudi Arabia.doi:10.1130/GES01625.1.
Downs D.T., Robinson J.E., Stelten M.E., Champion D.E., Dietterich H.R., Sisson T.W., Zahran H., Hassan K., Shawali J. 2019. Geologic map of the northern Harrat Rahat volcanic field, Kingdom of Saudi Arabia. 10.3133/sim3428.
Downs, D.T., Stelten, M.E., Dietterich, H.R., Champion, D.E., Mahood, G.A., Sisson, T.W., Calvert, A.T., & Shawali, J. (2023). Explosive trachyte eruptions from the Al Efairia volcanic center in northern Harrat Rahat, Kingdom of Saudi Arabia [Report] (1862G). (Professional paper, issue. U. S. G. Survey. https://pubs.usgs.gov/publication/pp1862G.
Dumas, P., Kumar, S., Martini, E., Vander Velde, M., 2023. EGEC Geothermal Marker Report 2022, 12th ed. EGEC - European Geothermal Energy Council. July 2023.
Duwiquet, H., Guillou-Frottier, L., Arbaret, L., et al., 2021. Crustal fault zones (CFZ) as geothermal power systems: a preliminary 3D THM model constrained by a multidisciplinary approach. Geofluids. https://doi.org/10.1155/2021/8855632.
Farahani, M.A., Gogolla, T., 1999. Spontaneous Raman scattering in optical fibers with modulated probe light for distributed temperature Raman remote sensing. J. Light. Technol. 17, 1379–1391. https://doi.org/10.1109/50.779159.
Flóvenz, Ó.G., Saemundsson, K., 1993. Heat flow and geothermal processes in Iceland. Tectonophysics 225, 123–138.
Frey, M., Bär, K., Stober, I., et al., 2022. Assessment of deep geothermal research and development in the Upper Rhine Graben. Geotherm. Energy 10, 18. https://doi.org/10.1186/s40517-022-00226-2.
Genter, A., Evans, K., Cuenot, N., Fritsch, D., Sanjuan, B., 2010. Contribution of the exploration of deep crystalline fractured reservoir of Soultz to the knowledge of Enhanced Geothermal Systems (EGS). C. R. Geosci. https://doi.org/10.1016/j.crte.2010.01.006.
Gustafsson, S.E., 1991. Transient plane source techniques for thermal conductivity and thermal diffusivity measurements of solid materials. Rev. Sci. Instrum. 62 (3), 797–804. https://doi.org/10.1063/1.1142087.
Hakala, P., Vallin, S., Arola, T., Martinkauppi, I., 2021. Novel use of the enhanced thermal response test in crystalline bedrock. Renew. Energy 182 (2022), 467–482. https://doi.org/10.1016/j.renene.2021.10.020.
Heap, M.J.;., Kushnir, A.R.L., Vasseur, J., Wadsworth, J.B., Harlé, P., Baud, P., Kennedy, B.M., Troll, V.R., Deegan, F.M., 2020. The thermal properties of porous andesite. J. Volcanol. Geotherm. Res. 398. https://doi.org/10.1016/j.jvolgeores.2020.106901.
Holford, S., Schofield, N., Bunch, M., Bischoff, A.P., Swierczek, W., 2021. Storing CO2 in buried volcanoes. APPEA J. 61, 1–6. https://doi.org/10.1071/AJ20056.
Jahnke, C., Wannous, M., Troeger, U., Falk, M., Struck, U., 2019. Impact of seawater intrusion and disposal of desalinization brines on groundwater quality in El Gouna, Egypt, Red Sea Area. Process analyses by means of chemical and isotopic signatures. Appl. Geochem. 100 (2019), 64–76. https://doi.org/10.1016/j.apgeochem.2018.11.001. PagesISSN 0883-2927.
Jolie, E., Scott, S., Faulds, J., et al., 2021. Geological controls on geothermal resources for power generation. Nat. Rev. Earth. Environ. 2, 324–339. https://doi.org/10.1038/s43017-021-00154-y.
Incropera, F., DeWitt, D., Bergman, T., Lavinne, A., 2007. Fundamentals of Heat and Mass Transfer, 6th ed. John Wiley & Sons. Inc., p. 1070
Ledésert, B., Hebert, R., Genter, A., Bartier, D., Clauer, N., Grall, C., 2009. Fractures, hydrothermal alterations and permeability in the Soultz enhanced geothermal system. C. R. Geosci. 342, 7–8. https://doi.org/10.1016/j.crte.2009.09.011. Issues.
Johnson P.R., Halverson G.P., Kusky T.M., Stern R.J., Pease V. 2013. Volcanosedimentary basins in the Arabian-Nubian shield: markers of repeated exhumation and denudation in a neoproterozoic accretionary orogen. 10.3390/geosciences3030389.
Kamboj, Puneet, Hejazi, Mohamad, Alhadhrami, Khalid, Qiu, Yang, Kyle, Page, Iyer, Gokul, 2023. Saudi Arabia Net Zero GHG Emissions by 2060: Transformation of the Electricity Sector. King Abdullah Petroleum Studies and Research Center (KAPSARC), Riyadh.
Kelkar, S., WoldeGabriel, G., Rehfeldt, K., 2016. Lessons learned from the pioneering hot dry rock project at Fenton Hill, USA. Geothermics 63. https://doi.org/10.1016/j.geothermics.2015.08.008.
Khodayar, M., Björnsson, S., 2024. Conventional geothermal systems and unconventional geothermal developments: an overview. Open J. Geol. 14, 196–246. https://doi.org/10.4236/ojg.2024.142012.
Kraal, K., Ayling, B.F., Blake, K., Hackett, L., Perdana, T.S.P., Stacey, R., 2021. Linkages between hydrothermal alteration, natural fractures, and permeability: integration of borehole data for reservoir characterization at the Fallon FORGE EGS site, Nevada, USA. Geothermics 89. https://doi.org/10.1016/j.geothermics.2020.101946.
Kukkonen, I., Heikkinen, P.J., Malin, P.E., Renner, J., Dresen, G., Karjalainen, A., Rytkönen, J., Solantie, J., 2023. Hydraulic conductivity of the crystalline crust: insights from hydraulic stimulation and induced seismicity of an enhanced geothermal system pilot reservoir at 6 km depth, Espoo, southern Finland. Geothermics 112. https://doi.org/10.1016/j.geothermics.2023.102743.
Langenheim V.E., Ritzinger B.T., Zahran H., Shareef A., Al-dahri M. 2018. Crustal structure of the northern Harrat Rahat volcanic field (Saudi Arabia) from gravity and aeromagnetic data. 10.1016/j.tecto.2018.11.005.
Lashin et al. 2020. A review of the geothermal resources of Saudi Arabia: 2015-2020.
Lucazeau, F., 2019. Analysis and mapping of an updated terrestrial heat flow data set. Geochem. Geophys. Geosyst. 20, 4001–4024.
Martinkauppi, A., Piipponen, K., 2022. Geothermal energy modelling of medium-deep boreholes in a sedimentary formation with crystalline basement. In: Proceedings of the European Geothermal Congress 2022. Berlin, Germany, p. 9, 17–21 October 2022.
Millett, J.M., Rossetti, L., Bischoff, A.P., Rossetti, M., Rosenqvist, M.P., Avseth, P., Hole, M.J., Pierdominici, S., Ealy, D., Jerram, D.A., Planke, S., 2023. Lava flow hosted reservoirs: a review. Geol. Soc. 547. https://doi.org/10.1144/Sp547-2023-102. London, Special Publications.
Moufti, M.R., Németh, K., 2016. Harrat Rahat: the geoheritage value of the youngest long-lived volcanic field in the Kingdom of Saudi Arabia. M. R. Moufti & K. Németh (Eds.). Geoheritage of Volcanic Harrats in Saudi Arabia. Springer International Publishing, pp. 33–120. https://doi.org/10.1007/978-3-319-33015-0_3.
Murcia, H., Németh, K., Moufti, M.R., Lindsay, J.M., El-Masry, N., Cronin, S.J., Qaddah, A., Smith, I.E.M., 2014. Late Holocene lava flow morphotypes of northern Harrat Rahat, Kingdom of Saudi Arabia: implications for the description of continental lava fields. J. Asian Earth. Sci. 84, 131–145. https://doi.org/10.1016/j.jseaes.2013.10.002.
Murcia, H.F., Lindsay, J.M., Németh, K., Smith, I.E.M., Cronin, S.J., Moufti, M.R.H., El-Masry, N.N., Niedermann, S., 2016. Geology and Geochemistry of Late Quaternary Volcanism in Northern Harrat Rahat, Kingdom of Saudi Arabia; Implications For Eruption dynamics, Regional Stratigraphy and Magma Evolution, 446. Special Publication - Geological Society of London, pp. 173–204, 132.
Németh, K., Kereszturi, G., 2015. Monogenetic volcanism: personal views and discussion. Int. J. Earth Sci. 104 (8), 2131–2146. https://doi.org/10.1007/s00531-015-1243-6.
Nishimoto, S., Yoshida, H., 2010. Hydrothermal alteration of deep fractured granite: effects of dissolution and precipitation. Lithos 115, 1–4. https://doi.org/10.1016/j.lithos.2009.11.015. Issues.
Norbeck J.H., Latimer T.M. 2023. Commercial-scale demonstration of a first-of-a-kind enhanced geothermal system. EarthArXiv Pre-print. 10.31223/X52X0B.
Pellaton C. 1981. Geologic map of the Al Madinah quadrangle, sheet 24D, Kingdom of Saudi Arabia: saudi Arabian Directorate General of Mineral Resources Geologic map GM-52C, scale 1:250,000, 19 p.
Piipponen, K., Martinkauppi, A., Korhonen, K., Vallin, S., Arola, T., Bischoff, A., Leppäharju, N., 2022. The deeper the better? A thermogeological analysis of medium-deep borehole heat exchangers in low-enthalpy crystalline rocks. Geotherm. Energy 10, 12. https://doi.org/10.1186/s40517-022-00221-7.
Powers R.W., Ramirez Leon F., Redmond C.D., Elberg Jr E.L. 1963. Geology of the Arabian Peninsula: sedimentary Geology of Saudi Arabia. https://pubs.usgs.gov/pp/0560d/report.pdf.
Reinecker, J., Gutmanis, J., Foxford, A., Cotton, L., Dalby, C., Law, R., 2021. Geothermal exploration and reservoir modelling of the United Downs deep geothermal project, Cornwall (UK). Geothermics 97. https://doi.org/10.1016/j.geothermics.2021.102226.
Roobol M.J., Bankher K., Bamufleh S. 1995. Geothermal anomalies along the MMN Volcanic Line including the cities of Al Madinah al Munawwarah and Makkahal Mukarramah. Saudi arabian Deputy Ministry for Mineral Resources confidential report DMMR-MADINAH-CR-15-2.
Roobol, M.J., Al-Rehaili, M., Al-Zahrani, M.I., & Turkestani, A. (1997). An 11-km-long fissure system on northern Harrat Rahat, near the city of Al Madinah. Technical Report, BRGM-TR-97-17, 14.
Runge, M.G., Bebbington, M.S., Cronin, S.J., Lindsay, J.M., Moufti, M.R., 2016. Integrating geological and geophysical data to improve probabilistic hazard forecasting of Arabian Shield volcanism. J. Volcanol. Geotherm. Res. 311, 41–59. https://doi.org/10.1016/j.jvolgeores.2016.01.007.
Stein M. and Hofmann A.W. 1992. Fossil plume head beneath the Arabian lithosphere? doi:10.1016/0012-821X(92)90161-N.
Stern R.J. 1985. The Najd Fault System, Saudi Arabia and Egypt: a late precambrian rift-related transform system? 10.1029/TC004i005p00497.
Stern R.J. and Johnson. 2010. Continental lithosphere of the Arabian plate - A geologic, petrologic, and geophysical synthesis. 10.1016/j.earscirev.2010.01.002.
Toews, M., Holmes, M., 2021. Eavor-Lite performance update and extrapolation to commercial projects. GRC Trans. 45, 86–109.
Tsukamoto, S., Tagami, T., Zwingmann, H., 2020. Direct dating of fault movement. Understanding Faults. Elsevier, pp. 257–282. https://doi.org/10.1016/B978-0-12-815985-9.00007-2 edited by D. Tanner and C. Brandes.
Stelten, M.E., Downs, D.T., Champion, D.E., Dietterich, H.R., Calvert, A.T., Sisson, T.W., Mahood, G.A., Zahran, H., 2020. The timing and compositional evolution of volcanism within northern Harrat Rahat, Kingdom of Saudi Arabia. Bull. Geol. Soc. Am. 132 (7–8), 1381–1403. https://doi.org/10.1130/B35337.1.
Stelten, M.E., Downs, D.T., Champion, D.E., Dietterich, H.R., Calvert, A.T., Sisson, T.W., Mahood, G.A., & Zahran, H.M. (2023). Eruptive history of northern Harrat Rahat—Volume, timing, and composition of volcanism over the past 1.2 million years [Report](1862D). (Professional paper, issue. U. S. G. Survey. https://pubs.usgs.gov/publication/pp1862D.
Sanchez-Alfaro, P., Reich, M., Arancibia, G., et al., 2016. Physical, chemical and mineralogical evolution of the Tolhuaca geothermal system, southern Andes, Chile: insights into the interplay between hydrothermal alteration and brittle deformation. J. Volcanol. Geotherm. Res. 324. https://doi.org/10.1016/j.jvolgeores.2016.05.009.
Weydt, L.M., Lucci, F., Lacinska, A., et al., 2022. The impact of hydrothermal alteration on the physiochemical characteristics of reservoir rocks: the case of the Los Humeros geothermal field (Mexico). Geotherm. Energy 10 (20). https://doi.org/10.1186/s40517-022-00231-5.
Zatonski, V., Brown, C, 2023. Eavor-Lite U pdate after four years of operation. GRC Trans. 47.